A TRIDENT SCHOLAR PROJECT REPORT

NO. 463

Evaluation of Non-Oxide Fuel for Fission-based Nuclear Reactors on Spacecraft

by

Midshipman 1/C Dakota J. Allen, USN

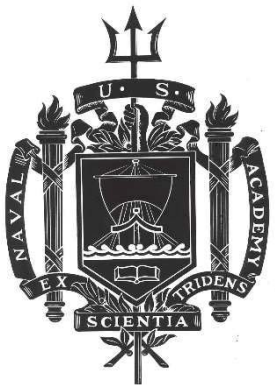

UNITED STATES NAVAL ACADEMY
ANNAPOLIS, MARYLAND

USNA-1531-2

REPORT DOCUMENTATION PAGE

Form Approved
OMB No. 0704-0188

1. REPORT DATE *(DD-MM-YYYY)*	**2. REPORT TYPE**	**3. DATES COVERED** *(From - To)*
05-21-18		

4. TITLE AND SUBTITLE
Evaluation of Non-Oxide Fuel for Fission-based Nuclear Reactors on Spacecraft

5a. CONTRACT NUMBER

5b. GRANT NUMBER

5c. PROGRAM ELEMENT NUMBER

6. AUTHOR(S)
Allen, Dakota J.

5d. PROJECT NUMBER

5e. TASK NUMBER

5f. WORK UNIT NUMBER

7. PERFORMING ORGANIZATION NAME(S) AND ADDRESS(ES)

8. PERFORMING ORGANIZATION REPORT NUMBER

9. SPONSORING / MONITORING AGENCY NAME(S) AND ADDRESS(ES)
U.S. Naval Academy
Annapolis, MD 21402

10. SPONSOR/MONITOR'S ACRONYM(S)

11. SPONSOR/MONITOR'S REPORT NUMBER(S)
Trident Scholar Report no. 463 (2018)

12. DISTRIBUTION / AVAILABILITY STATEMENT

This document has been approved for public release; its distribution is UNLIMITED.

13. SUPPLEMENTARY NOTES

14. ABSTRACT

The goal of this project was to study the performance of atypical uranium-based fuels in a nuclear reactor capable of producing 1 megawatt of thermal power with a 15-year core life for space-based applications. Specifically, the project investigated the use of uranium-molybdenum (UMo), uranium nitride (UN), or uranium carbide (UC) and compared their performance to uranium oxide (UO2) which is the fuel form used in the vast majority of commercial nuclear reactor applications. These alternative fuels have improved thermal conductivity and higher uranium loading density as compared to UO2. Improved thermal conductivity of the fuel allows a design with lower peak core temperatures thereby reducing the chance of violating thermal limits of core materials. Fuel with higher uranium loading density can have more of the fissile uranium-235 isotope present per unit of volume. This allows a design with a smaller and potentially lighter core, which is a significant advantage. The results of this study indicate that use of both UC and UN may result in significant weight savings due to higher uranium loading density. UMo is an effective fuel for use with low fuel burnup and low power applications. This study indicates that, due to restrictive operational temperature limits and adverse response to fission product gas buildup, UMo is inappropriate for designs requiring operation at high temperature, high power, and long duration such as is specified for the design under consideration.

15. SUBJECT TERMS
space, nuclear, fuel, non-oxide, MCNP

16. SECURITY CLASSIFICATION OF:			**17. LIMITATION OF ABSTRACT**	**18. NUMBER OF PAGES**	**19a. NAME OF RESPONSIBLE PERSON**
a. REPORT	**b. ABSTRACT**	**c. THIS PAGE**		103	**19b. TELEPHONE NUMBER** *(include area code)*

U.S.N.A. --- Trident Scholar project report; no. 463 (2018)

EVALUATION OF NON-OXIDE FUEL FOR FISSION-BASED NUCLEAR REACTORS ON SPACECRAFT

by

Midshipman 1/C Dakota J. Allen
United States Naval Academy
Annapolis, Maryland

_____
(signature)
Certification of Adviser(s) Approval

CDR Stuart Blair, USN
Mechanical Engineering Department

_____
(signature)

_____
(date)

Professor (ret) Martin Nelson
Mechanical Engineering Department

_____
(signature)

_____
(date)

Assistant Professor Marshall Millett
Mechanical Engineering Department

_____
(signature)

_____
(date)

Acceptance for the Trident Scholar Committee

Professor Maria J. Schroeder
Associate Director of Midshipman Research

_____
(signature)

_____
(date)

USNA-1531-2

Abstract

The goal of this project was to study the performance of atypical uranium-based fuels in a nuclear reactor capable of producing 1 megawatt of thermal power with a 15-year core life for space-based applications. Specifically, the project investigated the use of uranium-molybdenum (UMo), uranium nitride (UN), or uranium carbide (UC) and compared their performance to uranium oxide (UO_2) which is the fuel form used in the vast majority of commercial nuclear reactor applications. These alternative fuels have improved thermal conductivity and higher uranium loading density as compared to UO_2. Improved thermal conductivity of the fuel allows a design with lower peak core temperatures thereby reducing the chance of violating thermal limits of core materials. Fuel with higher uranium loading density can have more of the fissile uranium-235 isotope present per unit of volume. This allows a design with a smaller and potentially lighter core, which is a significant advantage.

The results of this study indicate that use of both UC and UN may result in significant weight savings due to higher uranium loading density. A neutron transport analysis of the core shows that UN fuel was able to maintain a negative temperature coefficient of reactivity throughout core life with attendant safety benefits. UC, however, appears to not maintain a negative temperature coefficient of reactivity and thus may require additional reactor control mechanisms to maintain stable power output and safe operation. UMo is an effective fuel for use with low fuel burnup and low power applications. This study indicates that, due to restrictive operational temperature limits and adverse response to fission product gas buildup, UMo is inappropriate for designs requiring operation at high temperature, high power, and long duration such as is specified for the design under consideration.

Keywords: space, nuclear, fuel, non-oxide, MCNP

Acknowledgements

Conducting this study would not have been possible without the tireless commitment of my USNA advisers: CDR Stuart Blair, USN, Professor (ret) Martin Nelson, and Asst. Professor Marshall Millett all from the USNA Mechanical Engineering Department. In addition, I would like to thank Mark Natale from Naval Reactors who worked to get me proper information and to set up my Bettis Atomic Power Labs internship. The assistance these advisers have provided me in conducting this research has been paramount for me to tackle this topic. They have assisted me in learning the variety of unique conditions present within the core and have assisted in ensuring the work done is of the highest quality. I would not be able to do this study without their assistance and wisdom.

In addition to my advisers, I would not have been able to do this without the support of my internship mentors from the past two summers. These mentors include Dr. David Poston, LANL; Dr. Szelim Kong, Bettis Atomic Power Labs; Adam Daniel, Bettis Atomic Power Labs; Dr. Dave Sottosanti, Bettis Atomic Power Labs; and Dr. Tim Goorley, LANL. These industry professionals have provided excellent support and knowledge to me over the last two years to inspire me and show me the real world application of research.

Other people I would also like to thank, include the Trident Committee for their support in my research and time spent reviewing the material. I would like to thank DTRA for providing funds for me to attend my internship at LANL. Lastly, I would like to thank anybody who has assisted me behind the scenes without my knowledge, to include any IT assistance or planning of my internships.

Table of Contents

List of Figures

List of Tables

Technical Nomenclature

1 kWe	1,000 watts of electric power
1 kWt	1,000 watts of thermal power
1 MWt	1,000,000 watts of thermal power
A	Cross sectional area
ASTAR-811C	Tantalum, Tungsten, and Rhenium based Refractory Alloy
at%	Atomic Percent
B_4C	Boron Carbide
BAPL	Bettis Atomic Power Laboratory
BeO	Beryllium Oxide
BOL	Beginning of Life
CTE	Coefficient of Thermal Expansion
E	Energy generated in Pin
EOL	End of Life
FS-85	Niobium and Tantalum based Refractory Alloy
gU/cc	Grams of uranium per volume

h	Height on Page 36 Heat Transfer Coefficient on Page 31
h_c	Convection Heat Transfer Coefficient of Coolant ($\frac{W}{cm^2\ K}$)
h_g	Convection Heat Transfer Coefficient of Gap ($\frac{W}{cm^2\ K}$)
Haynes 230	Nickel Based Superalloy
HeXe	Helium Xenon Mixture
K	Degrees Kelvin
k	Thermal Conductivity ($\frac{W}{cm\ K}$)
k_c	Thermal Conductivity of Clad ($\frac{W}{cm\ K}$)
k_f	Thermal Conductivity of Fuel ($\frac{W}{cm\ K}$)
k_l	Thermal Conductivity of Liner ($\frac{W}{cm\ K}$)
k_{eff}	Effective Multiplication Factor
k_{eff1}	Effective Multiplication Factor of Case 1
k_{eff2}	Effective Multiplication Factor of Case 2
kg	Mass in kilograms
kg/m^3	Density (mass per volume)

m	Mass of the fuel pin
MCNP	Monte Carlo N-Particle
Mo	Molybdenum
Mo-47.5Re	47.5 wt% Rhenium and 52.5 wt% Molybdenum
MOL	Middle of Life
N	Number of fuel pins
PCT	Peak Core Temperature (K)
PF	Peaking Factor
Q	Necessary Heat generation
q_{in}	Heat into Gap ($\frac{W}{cm}$)
q_{out}	Heat exiting Gap ($\frac{W}{cm}$)
q′	Linear Heat Rate ($\frac{W}{cm}$)
q″	Heat Flux ($\frac{W}{cm^2}$)
q‴	Volumetric Heat Generation ($\frac{W}{cm^3}$)
r	Radius (cm)
r_f	Outer Radius of Fuel (cm)
r_i	Inner Radius (cm)

r_o	Outer Radius (cm)
Re	Rhenium
RERTR	Reduced Enrichment for Research and Test Reactors
SF	Scaling factor
T	Temperature of Core
t	Time
T_1	Temperature of Case 1
T_2	Temperature of Case 2
T_{PCT}	Peak Core Temperature (K)
T_b	Bulk Coolant Temperature (K)
T_{ocl}	Temperature of Outer Radius of Clad (K)
T_{of}	Temperature of Outer Radius of Fuel (K)
T_{og}	Temperature of Outer Radius of Gap (K)
T_{ol}	Temperature of Outer Radius of Liner (K)
t_{cl}	Thickness of Clad (cm)
t_{co}	Thickness of Coolant (cm)
t_g	Thickness of Gap (cm)

t_l	Thickness of Liner (cm)
U-10Mo	Uranium Mo fuel with 10 weight percent Mo
$^{234/235/238}$U	Uranium 234, 235, and 238
UC	Uranium Carbide Fuel
UMo	Uranium Molybdenum Fuel
UN	Uranium Nitride Fuel
z	Height of the fuel pin
α_T	Temperature Coefficient of Reactivity
α_T	Temperature Coefficient of Reactivity (/K)
ρ	Reactivity
φ	Average Neutron Flux

1 Background

In order to better understand the concepts behind this research, the basics of nuclear reactors, nuclear fuel, and core analysis will be reviewed. Section 1.1 will begin by discussing the fundamental physics of nuclear reactors. Section 1.2 will discuss the logic behind alloying fuel material and why the fuels analyzed in this study differ. Lastly, Section 1.3 will briefly describe the analysis method.

1.1 Nuclear Reactors

Nuclear reactors are just another method of providing heat to an energy conversion system based on, for example, a Rankine cycle or a Brayton cycle. The nuclear reactor generates heat through the process of fission in which fissionable isotopes (contained in the fuel) absorb an incident neutron and subsequently split. Isotopes that undergo fission when absorbing energetic neutrons (^{238}U, ^{235}U and ^{239}Pu) are termed "fissionable" while those isotopes that also fission when absorbing a neutron with low energy (^{235}U and ^{239}Pu) are termed "fissile". By splitting, the fuel atom divides into two or more fission products; the kinetic energy of these fission products dissipates into thermal energy in surrounding fuel material. The fission process also results in the liberation of a small number of neutrons—on average between two or three per fission event—some of which can initiate, in turn, a chain reaction of such fission events. The thermal energy deposited in surrounding fuel material is transported to cooling fluid that delivers the energy to a conversion system. Details of the energy conversion system are not within the scope of this study. The analysis is based on a core consisting of cylindrical fuel pins using 93% enriched uranium fuel with the fissile isotope being uranium-235 (^{235}U) and a helium-xenon mixture as the gas coolant.

Fission-based nuclear reactors can roughly be divided into two categories; those in which the fission events are predominantly initiated by high energy neutrons—termed "fast" reactors—and those in which the fission events are predominantly initiated by slow, or thermal, energy neutrons – termed thermal reactors. Reactors of this latter type have an extra component called the moderator; a material with a low atomic mass such as graphite or water that interacts with high-energy neutrons through scattering interactions; gradually slowing down the neutrons until their energy is comparable to the thermal energy of the nuclei of the moderating material. Fast reactors may have compact cores with fuel that is highly enriched in fissile isotopes. Thermal reactors typically have larger core regions with volume available for the moderator material to slow down neutrons as they transport through the core. A characteristic common among all fissile materials is that interactions with neutrons resulting in fission are much more likely when the incident neutron is of low energy. For this reason, thermal reactors can also use fuel that is of low enrichment. Due to the fact that fast fission reactors may be more compact, they make ideal candidates for space missions as the extra weight of a moderator would make launching the reactor more difficult. The subject of this study is a fast fission reactor.

The power output of a nuclear reactor is controlled by managing the population of neutrons in the core. Of all neutrons produced in a fission event, some will transport beyond core boundaries (termed "leakage") and be unable to initiate follow-on fission events. Others may be absorbed by non-fissile isotopes present within the core or be absorbed by a fissile fuel isotope in a non-fission capture and be lost. Collectively, the average number of neutrons born from each fission event that go on to cause a follow-on fission event is referred to as the effective multiplication factor, k_{eff}, and is an indicator of the stability of core power level. If the reactor

k_{eff} is equal to unity (1 neutron for every fission occurring), the reactor is "critical". The fractional deviation of k_{eff} from unity is called reactivity.

The design of any reactor must also provide for control of reactivity. The design under consideration uses materials to control reactivity in two ways: a reflector and a safety control rod. The reflector is a material installed at the periphery of the core that can interact with leaking neutrons and re-direct them back into the core; in this way, they add positive reactivity and increase k_{eff}. Reflector material must have high atom density—to make scattering interactions with neutrons probable—but low probability of absorbing a neutron. A set of wedge-shaped beryllium oxide plates placed outside the periphery of the reactor meet these criteria and are used as a reflector for this core design. The safety control rod is made with a material that has high probability of absorbing neutrons. By positioning the safety control rod in the core, k_{eff} can be reduced—lowering reactivity. Reactivity can be increased again by withdrawing the safety rod. The design in this paper uses a boron carbide (B_4C) safety control rod designed principally as protection against a postulated accident during the launch to transport the reactor into space.

In addition to reactor materials causing changes in reactivity, the temperature of the reactor can affect its reactivity. The change in reactivity associated with each change in temperature is referred to as the temperature coefficient of reactivity (α_T). The sign of this value is important in evaluating the safety of the reactor as it determines whether the reactor will have positive or negative feedback due to changes in temperature. A positive α_T indicates that an increase in temperature will add positive reactivity to the core causing further increase in temperature. This can lead to violation of the thermal limits of core materials. A negative α_T means an increase in temperature will cause an addition of negative reactivity to the core,

reducing the fission rate and allowing the core power to follow the power demand in a stable manner.

1.2 Fuel Materials

In this study it is important to distinguish the different types of materials and why they are present in the core. The fuel for nuclear reactors is typically uranium. However, uranium is a reactive metal with a melting point of less than 1200 °C and the environment within nuclear reactor fuel is commonly above uranium's melting temperature. In order to prevent damage to the fuel, uranium is combined with different materials in order to improve its material properties. In the case of most commercial power plants, this material is oxygen, which makes uranium oxide (UO_2). This fuel is designed to survive the high temperatures of commercial nuclear power plants. Non-oxide fuels alloy uranium with a material other than oxygen, including nitrogen, carbon, and other metals such as molybdenum, all alloying materials being evaluated in this study. Uranium alloyed with these materials produces uranium nitride (UN), uranium carbide (UC), and uranium molybdenum (UMo).

1.3 Core Analysis

The analysis of this reactor model was accomplished using the Monte Carlo N-particle (MCNP) code. Input is provided to MCNP sufficient to describe the reactor geometry and material composition. MCNP uses statistical sampling to simulate successive generations of neutrons as they are generated in fission, transport through the core, and interact with core materials. Databases describing the probability of various interactions between neutrons and atoms that make up the core material—the probabilities of these interactions are called "cross sections"—govern neutron behavior from one interaction to the next. The code can produce a

variety of user-requested outputs; however, the principal parameter evaluated in this study is k_{eff}. Changes in core temperature, along with the subsequent changes in core material density and geometry can be evaluated for their impact on k_{eff}. The temperature of core materials directly impacts the previously mentioned cross section data through the Doppler broadening effect of resonance absorption, while the material density and geometry impact interactions through the atomic (or target) density.

As reactor operations create power through the process of fission, which destroys fuel atoms and creates fission product atoms—along with products of non-fission neutron interactions—the composition of a reactor core changes over time. MCNP is also used to estimate these changes in fuel composition over time.

Further details of how the output from the MCNP code is used to evaluate fuel performance are provided in section 2.

2 Overview

After gaining a better understanding of the concepts of the research, it is also important to understand the tools used in the research. Section 2.1 will discuss the reactor used in this evaluation and the variations used in the model. Section 2.2 will discuss the method of approach developed for analyzing the performance of the reactor models.

2.1 Reactor Model

This study utilizes a 1 MWt reactor that was designed for use in Project Prometheus [1]. There are nine main parts to the reactor core as shown in Figure 2.1; namely, the fuel, liner, gap, clad, coolant, fission spring, block, reflector and safety pin. The core is a combination of common unit cells that comprise many of these parts; a schematic of the reactor showing the core construction is provided in Figure 3.1 in section 3.1

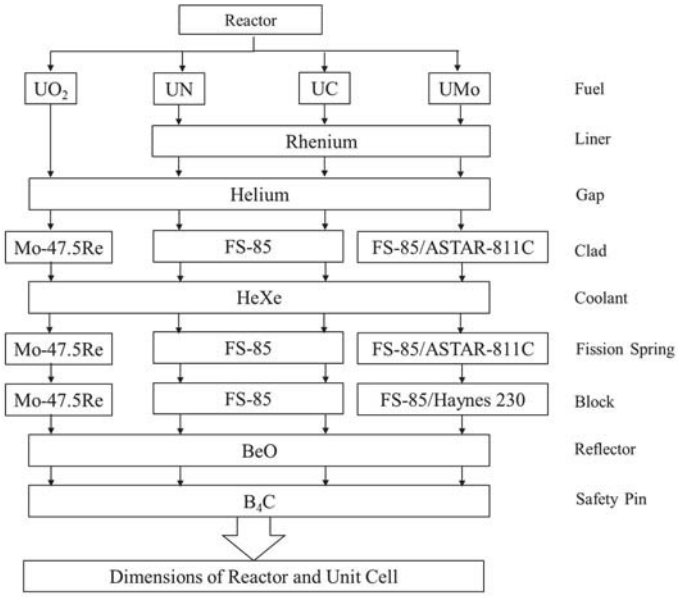

Figure 2.1: Reactor Model

The main focus of this research is to compare core performance with the various forms of the uranium fuel (UO_2, UN, UC, and UMo). The fuel pins that contain the fuel within the reactor

are surrounded by up to three protective buffers (i.e. liner, gap, and clad). The first layer of protection for most of the fuels is a liner, a solid metal sleeve that helps contain fission products. As shown in Figure 2.1, rhenium is the liner for UN, UC, and UMo. No liner is used for UO_2 because experience with its use has shown that it contains fission products sufficiently well. Outside of the liner is a gap that is filled with an inert gas, which is helium for all fuels. The gap exists to account for thermal expansion of the fuel and cladding. The gap is sized to prevent physical contact between the fuel and cladding. Such contact could result in localized stress and potential cladding failure. The clad serves to contain the fission products while also protecting the fuel from corrosion by the coolant. The clad varies between the non-oxide fuels and UO_2 due to the increased protection provided by the liner. UO_2 uses Mo-47.5Re for a clad, while the non-oxide fuels use FS-85. The one exception is UMo which may use ASTAR-811C depending on what coolant bulk temperature is reached. The coolant flows outside of the clad and transports the heat to the power generation cycle. In all models, the coolant was taken to be a mixture of helium and xenon.

In order to provide axial support to each fuel pin, springs are axially aligned with the fuel within the unit cell. These springs can be seen in Figure 3.1a below the fuel (Figure 3.1a is upside down relative to launch orientation) and serve to limit the amount of axial motion and stress caused to the fuel during the launch of the spacecraft.

The fuel pin is encased by the annular flow block. This block ensures the flow of coolant is distributed among all fuel pins evenly. The block material utilized for UO_2 is MO-47.5Re. In the non-oxide cases, FS-85 is used for all cases except for a special case of UMo. In the case that UMo uses ASTAR-811C as the clad, the block material can be Haynes 230 nickel alloy. Section 3.3 discusses more completely the considerations used in adopting the reactor block design.

The last elements of the reactor model are the reflectors and safety pin, which serve to help control the reactor power level. Reflectors are used to scatter neutrons back into the fuel. In order to change the reactor's power, the reflectors can be moved axially, which changes the neutron leakage at a rate corresponding to the axial variation in the neutron flux. The reflector consists of BeO for all fuel types. Moving the reflectors into a region with high axial flux increases the reactor power, while moving them away from high flux and toward lower axial flux decreases the reactor power. Another method of controlling the reactor is moving the safety pin that is contained at the center point of the reactor, as seen in Figure 3.1(a). This safety pin is made of B_4C for all fuel types, with boron being a strong neutron poison (or neutron absorber). This safety pin exists primarily to ensure a subcritical configuration during credible launch accidents, but could be used as a control mechanism, where moving it into a region of high axial flux would decrease the reactor power, the opposite effect as with the reflectors.

After identifying all the material options, the last step before applying the method of approach developed was to determine the dimensions of each reactor. The dimensions of the UO_2 fueled reactor (i.e. base case) were also taken from the design for Project Prometheus. This was done in order to provide a credible and feasible design for comparison. While each non-oxide reactor follows the general design of the base case, the dimensions of each non-oxide fuel reactor were changed in order to accommodate the changing material properties while maintaining consistent total ^{235}U load within the reactor.

2.2 Method of Approach

The initial part of this study was to develop a method of approach to examine this type of fast fission reactor in space. This process is shown with each steps' output in Figure 2.2 below.

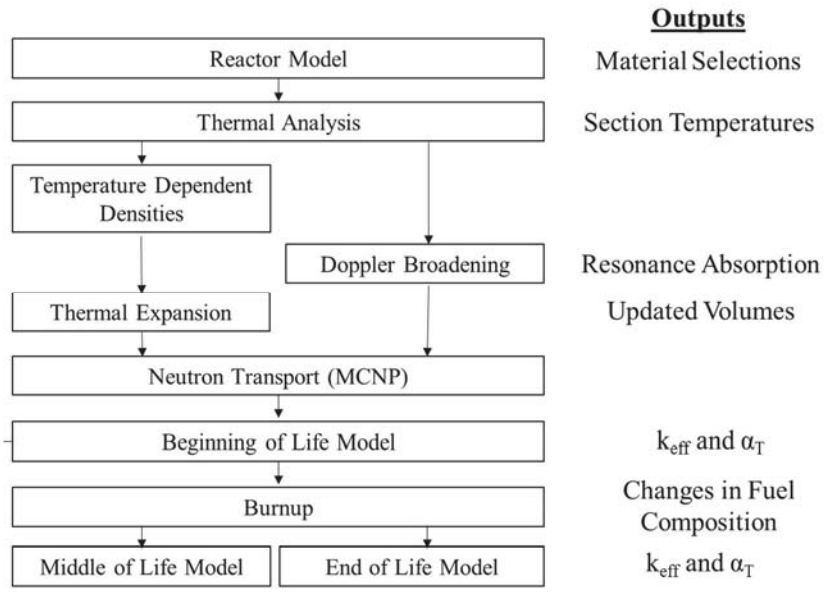

Figure 2.2: Method of Approach

This method begins by choosing one of the four fuel types, which leads to the materials and dimensions for the reactor as shown in Figure 2.1. The chosen material's thermal conductivity, system heat transfer coefficient, and dimensions are then used in the thermal analysis to calculate the temperatures within the unit cell as shown in Figure 3.1 for three different reactor power levels (1 MWt, 1.5 MWt, and 2 MWt; or peaking factors (PF) =1.0, PF=1.5, and PF=2.0). These temperatures are used to calculate new material densities due to thermal expansion as shown in section 4.3 and changes in neutron cross sections due to the Doppler broadening effect, which is discussed in section 4.4. Both of these effects change the neutron interaction rate and thus the reactor's k_{eff}. These temperature dependent densities are then used to calculate the change in component volume and dimensions as shown in the thermal expansion block in Figure 2.2.

The Doppler broadening temperature correction is the effect that increased temperature has on the vibrational energy of the atoms within the lattice structure of the material. As

temperature increases, these atoms become excited, thus increasing their vibrational energy. Neutron absorption probabilities show peaks at energy resonances where the resonance energy is actually a combination of the kinetic energy of both neutron and nucleus. As the vibrational energy of a nucleus increases, the range of neutron-nucleus combinations that result in the resonance energy increases, allowing more neutrons to experience the resonance, and ultimately increasing the neutron absorption in the material, thus change the reactor's k_{eff}.

Thermal expansion and Doppler broadening effects are then integrated into to an MCNP (Monte Carlo N-Particle Code) neutron transport model. Thermal expansion is applied to this model by providing updated dimensions and densities in the cell section and surface section of the code as shown in Appendix A, lines 10-900 and the material section of the code. Doppler broadening is incorporated into the model by calculating updated material cross section data corresponding to the estimated material temperature. Cross sections for all materials are evaluated at several discrete points spanning the temperature range of interest. MCNP is distributed with a utility program that accomplishes this task. The MCNP input is subsequently modified to use the new cross section data, which is further explained in section 4.4. After thermal expansion and Doppler broadening are applied for all three power levels at the beginning of life (BOL) of the reactor, this model is used for Middle of Life (MOL or 7.5 years of use) and End of Life (EOL or 15 years of use). In addition to analyzing the reactor at three different powers, the reactor is also analyzed at room temperature using the initial baseline conditions that include MCNP's default resonance absorption conditions.

Burnup is the term used to describe changes in nuclear fuel composition over time. Fuel atoms are destroyed in the fission process. The resulting fission products are typically unstable and are subject to radioactive decay processes that result in the creation of still more atomic

species. Beyond burnup through fission, fuel materials are changed through non-fission neutron absorption (capture) reactions. This process is referred to as transmutation. Some of these transmutation processes result in the production of isotopes that are significant from the perspective of the core physics model. For example, radiative capture in ^{238}U produces isotopes that in a few days decay into ^{239}Pu, which is fissile. The population of these new isotopes within the core must be updated in a burnup calculation as they also affect the value of overall k_{eff}. Typically, the cumulative effect of burnup of fuel will cause the value of k_{eff} to decrease slowly over lifetime due to the consumption of fuel atoms and the build-up of fission product atoms, many of which are neutron absorbers.

The burnup calculations were done using MCNP to determine the concentration of isotopes within the fuel at MOL and EOL, and then these isotopic concentrations were used in the MOL and EOL analyses of k_{eff} and α_T. These analyses were conducted using the effect of thermal expansion and Doppler broadening at three power levels and room temperature in the same way as done in the BOL analysis, only with different fuel isotopic concentrations. The values of the MOL and EOL analyses were compared to that of BOL in order to evaluate how the reactor's k_{eff} and α_T change over lifetime. These burnup analyses are provided in sections 4.7 and 4.8 for UO_2, section 6.3 for UN, and section 7.3 for UC.

3 Model Development

This part of the report focuses on how each reactor model used for the fuel analyses was designed and chosen. Section 3.1 will discuss the overall design of the reactor. Section 3.2 will discuss the choices for materials in the core other than the fuel itself, including clad, block, and liner material. Section 3.3 will discuss the reasoning behind the geometry chosen in different areas of the reactor.

3.1 Design Concepts

The first step in this study was to gain a further understanding of the space reactor being studied. In order to accomplish this, an internship was completed at Bettis Atomic Power Laboratory (BAPL) in Pittsburgh, PA, one of the labs utilized by Naval Reactors to conduct research for the Navy. When NASA asked Naval Reactors in 2003 to assist with the Project Prometheus program, Naval Reactors tasked BAPL to design a reactor that could fit the mission set [2]. Through this exercise, as well as their design work for the Navy, BAPL gained expertise in the space reactor domain. Through this internship, assistance was provided to this project directly through interaction with the design experts and also through the provision of Project Prometheus documentation. The interactions and documentation at BAPL provided this project with a comprehensive view of the entire design process and why certain choices were made.

The most important part of this internship experience was gaining an understanding of the design choices made during the study. One of these was to make the reactor a fast fission reactor. BAPL material choices for Project Prometheus are discussed in section 4.2, while the core geometry description is given in section 4.3. This original design was used as the basis for

the base case study given in section 4. A visualization of this design and the fuel pin can be seen in Figure 3.1.

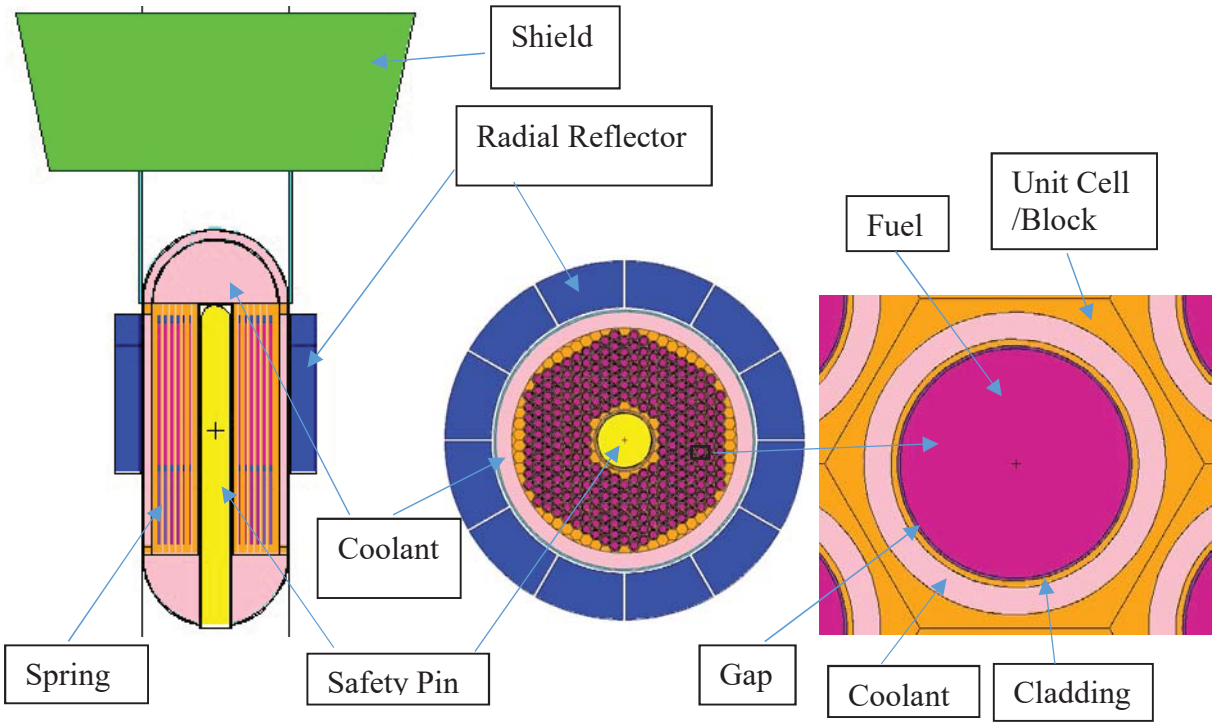

Figure 3.1: (a) Axial View of Reactor (b) Radial View of Reactor (c) Fuel Pin within the Unit Cell with no liner

3.2 Material Choices

From the beginning, it was understood that the likelihood of degrading interaction between materials, such as corrosion or radiation damage, would be a challenging part of this study. The first step in understanding Project Prometheus was to understand the reasoning behind many of the material choices that were made in the reactor design. These choices included specific precautions taken in regard to the environment of space. For a nuclear reactor to be safely launched, then reach and operate in space, it must be able to withstand extreme conditions. One of these is a malfunction during launch, which could lead to the reactor crashing into sand land or water. This is a scenario in which a fast fission reactor would be in the sudden presence

of a moderator, causing an increase in neutron thermalization. Because thermal neutrons are much more likely to interact with fuel nuclei and induce fission, the sudden increase in a thermal neutron population results in a corresponding increase in k_{eff} and may result in a subcritical assembly becoming critical. To mitigate this risk, structural materials for the reactor were chosen that would preferentially absorb thermal neutrons versus the fast neutrons needed for operation. Materials with this property are referred to as spectral shift poisons [3]. One category of materials that has this capability is refractory alloys [4].

While spectral shift poisons do not have a large negative effect on the fast neutron population vital to stable operation, they still have a small effect and the strength and amount must be controlled for each type of fuel. Due to this, each fuel type must be evaluated with the necessary amount of spectral shift poisons present in the core. As rhenium is the strongest spectral shift poison among refractory metals, alloys with high amounts of it will provide the greatest amount of thermal neutron absorption [4]. The refractory alloys in this study are contained within the liner (if applicable), the clad, and the block as seen in Figure 3.1. Table 3.1 below shows the refractory materials chosen by fuel type for the reactor's block and fuel's clad and liner. As can be seen in this table, UO_2 has no liner.

Table 3.1: Refractory Alloys designated for each Fuel

Fuel	Block	Clad	Liner
UO_2	Mo-47.5Re	Mo-47.5Re	N/A
UN	FS-85	FS-85	Re
UMo	FS-85/Haynes 230	FS-85/ASTAR-811C	Re
UC	FS-85	FS-85	Re

A rhenium (Re) liner was chosen for all fuels except UO_2 and this decision affected the materials chosen for the block and clad. A liner is present immediately outside the fuel (if

applicable) and serves to prevent the fission products from migrating through the clad and into the coolant. In commercial fuel (UO_2), fission products scavenge oxygen to form oxides, which reduces their mobility. Fission products are not as susceptible to bonding in non-oxide fuels that contain alloying materials (N, C, etc.) and hence have greater mobility, which necessitates the need for a liner. The UO_2 base case did not employ a liner so the block and clad used Mo-47.5Re, an alloy that has 47.5 percent by weight rhenium and the remainder being molybdenum. The fuels UN and UC need to have rhenium in the liner to ensure safety during launch accidents so they only require moderate strength poison in the block and clad, with niobium based FS-85 being a good choice. UMo is unique as it still needs a liner and could use the same poisons as UN. However, since its operating temperature is much lower than UN, it can use lower grade materials in the block, such as Haynes 230, a nickel-based superalloy that is much lighter and can survive within the core at a lower operating temperature [5]. However, Haynes 230 does not contain a sufficient amount of refractory metals needed to serve as a spectral shift poison. If Haynes 230 were to be used for the block, then the clad would need to be a strong poison, thus ASTAR-811C was chosen. ASTAR-811C is a refractory alloy that is tantalum-rich and includes rhenium, each good spectral shift poisons [6]. UC would be expected to have similar liner, clad and block materials as UN as shown in Table 3.1.

3.3 Core Geometry

Much of this study was balancing innovation with established practices. Note that his study only considers feasibility from a limited perspective, and much testing of non-oxide fuels will be necessary prior to the deployment of a non-oxide core. For this study, it was decided that all fuels would utilize the same geometry, making the comparison more focused on the differences between the fuels rather than the geometry. The main geometry decision for this

study was to utilize a modular annular flow block over an open lattice structure. An annular flow block is a large metal cylinder with a hole for each fuel pin drilled through it in the axial direction. The fuel pins are placed in the block, and this provides support to the fuel pins as well as a heat sink during transients. In a modular annular flow block, each fuel pin can be modeled within a unit cell, a section of the block that contains the coolant channel and other parts of the fuel pin. All of the unit cells together form a block and have the same neutronic response effects as a block, but are easier to construct than the whole block. An open lattice, a design that uses only fuel pins with no block for support, suffers from a lack of structure in the core. This lack of structure could lead to failure of the core as any lateral vibration of the fuel is not supported, and lateral displacement could cause mechanical failure or thermal failure in the case of permanent displacement. This is especially important due to the lower maximum allowable temperatures of non-oxide fuels. Due to this, the modular annular flow block was chosen for all fuel types even though it was much heavier than the open lattice structure. Thus, the major difference between each fuel evaluated was in the materials and dimensions that composed the reactor.

4 UO_2 Fueled Reactor (Base Case)

This section discusses the process of developing the base case UO_2 reactor. Section 4.1 begins by discussing the differences between oxide and non-oxide fuels and why these material properties can be beneficial. Section 4.2 discusses the thermal analysis completed and how temperatures were found at various points in the unit cell. Section 4.3 discusses how these temperatures are used in the calculation of the thermal expansion. Section 4.4 discusses the effect Doppler broadening has on the reactor and how to calculate it. Lastly, Section 4.5 presents the results of the base case beginning of life neutron transport model.

4.1 Material Properties

The differences between oxide fuels and non-oxide fuels reside in the material properties. Two specific material properties where non-oxide fuels have an advantage over oxide fuel is in loading density and thermal conductivity. Loading density is how much uranium fuel can be added while maintaining the same volume. It is important for this value to be high as this allows for a more compact core with attendant benefits to overall system weight. Non-oxide fuels have a lower amount of alloying material and thus are able to have a higher loading density. The values for uranium loading density of all fuels are shown in Table 4.1 below. In this table, U-10Mo means that Mo is 10 weight percent of the fuel.

Table 4.1: Loading Density of Fuels [7]

Fuel	Loading Density (gU/cc)
UO_2	8.26
UN	13.52
UC	12.97
U-10Mo	16.9

As seen in Table 4.1, each of the non-oxide fuels have a loading density that is at least 50% higher than that of UO_2. This allows the non-oxide fuel to deliver the same amount of uranium with a smaller volume and mass, making it easier to launch such a reactor into space. In addition to loading density, non-oxide fuels benefit from a higher thermal conductivity. Thermal conductivity is the measure of how much heat can pass through a material per distance for a given temperature change. The higher the value of thermal conductivity, the more heat that can pass through the material for the given temperature change. This is important as this property affects what the temperature will be at the centerline of the fuel, which is typically the hottest portion of the fuel. This temperature is defined as the peak core temperature (PCT), and a lower peak core temperature can lead to a safer reactor due to the less likelihood of melting or dissociation within the fuel. The thermal conductivities of the various fuels are indicated in Table 4.2.

Table 4.2: Thermal Conductivities of Fuels [7] [8] [9]

Fuel	Thermal Conductivity ($\frac{W}{cmK}$)
UO_2	0.03
UN	0.23
UC	0.25
U-10Mo	0.27

It is seen in Table 4.2 that the non-oxide fuels under consideration have thermal conductivities approximately an order of magnitude above that of UO_2, allowing these fuels to have a much lower temperature gradient across the fuel. This lower temperature gradient will allow for lower peak core temperature.

While non-oxide fuels benefit from having higher loading density and thermal conductivity, these fuels have lower maximum allowable temperatures. Maximum allowable temperature is not the melting temperature of a fuel, but rather the highest temperature the fuel can be used. Fuels, at temperatures sometimes much lower than the melting temperature, can begin to experience phase dissociations. Phase dissociations are when the uranium and the alloying material begin to separate. This will cause the uranium, now with the properties of just metallic uranium, to likely melt and cause severe damage to the fuel. Due to these phase dissociations, the maximum allowable temperature cannot be reached in order to maintain the integrity of the fuel. UO_2 was designed for commercial power plant use and has a very high maximum allowable temperature, surpassing that of the non-oxide fuels. The maximum allowable temperature of the fuels used in this study are provided in Table 4.3 below.

Table 4.3: Maximum Allowable Temperature of Fuels [8] [2]

Fuel	Maximum Allowable Temperature (K)
UO_2	1800
UN	1600
UC	~1600
U-10Mo	750

4.2 Thermal Analysis

One of the first steps to analyzing the fuels at 100 % power (1 MWt) was to conduct a thermal analysis of the fuel pin. This analysis produced the temperatures of different materials throughout the fuel pin. An important assumption made in the thermal analysis was that the coolant would remain at an 1150 K along the entire length of the fuel pin. This assumption of constant radial temperature applies to all the other sections of the fuel pin (i.e. fuel, pin, gap, etc.) at their specific calculated temperature. The reason for this assumption is that the core model

employed with MCNP does not discretize any of the core materials in either the radial or axial directions; the fuel comprises one region; a fuel pin gap the next; the same is true of the coolant and block. Consequently the MCNP model would not have been able to use more refined temperature estimates to obtain a more accurate neutron transport result. Results so far suggest that a more refined temperature analysis would produce a result with the same qualitative trends. Furthermore, the coarse handling of core temperature distribution used here is in-line with standard practice for projects of this scope and was employed by Bettis Atomic Power Laboratory when designing Project Prometheus.

Another assumption was to ignore the heat transfer in the axial direction. This was done because the height of the fuel is much larger than the fuel radius. Thermal conductivity was also assumed to be constant throughout the fuel instead of variable with the temperature. Lastly, the reactor was assumed to be at steady state. After making these assumptions, the next step was to derive equations for each section of the fuel pin: the fuel, liner, gap, clad, and coolant. This derivation was done beginning with equations 4.1 and 4.2 below [10]. These equations use 3 different forms of heat: q′, the linear heat rate along the axis, q″, the heat flux across the area of a surface, and q‴, the heat generated per a specific volume.

$$\frac{-1}{r}\frac{d}{dr}\left(kr\frac{dT}{dr}\right) = q'''(r) \tag{4.1}$$

$$q'' = \frac{q'}{2\pi r} = h(T_o - T_i) \tag{4.2}$$

Equations 4.1 and 4.2 are the conductive and convective heat transfer equations respectively. Equation 4.1 was used for sections of the fuel pin that employ solid materials. These sections include the fuel, cladding, and unit cell/block as seen in Figure 3.1c. The equation utilizes the thermal conductivity (k) and the heat generated in that section to calculate the

temperature gradient. Equation 4.2 was used for sections that contained a fluid. These sections include the gap and coolant also as seen in Figure 3.1c. A different equation was necessary as heat is removed from the fluid by convection, where h is the fluid's heat transfer coefficient, which allows for greater heat transfer than just conduction.

4.2.1 Derived Equations

In order to calculate the temperature gradients and temperatures of the desired sections, equations 4.1 and 4.2 were integrated across each section of the unit cell. The resulting equations are shown in Table 4.4 below.

Table 4.4: Thermal Analysis Equations

Section	Equation
Fuel	$T_{PCT} - T_{of} = \frac{q'}{4\pi k_f}$
Liner	$T_{of} - T_{ol} = \frac{q'}{2\pi k_l} * \ln\frac{r_f + t_l}{r_f}$
Gap	$T_{ol} - T_{og} = \frac{q'}{2\pi h_g(r_f + t_l)} - \frac{q'}{2\pi h_g(r_f + t_l + t_g)}$
Clad	$T_{og} - T_{ocl} = \frac{q'}{2\pi k_c} * \ln\frac{r_f + t_l + t_g + t_{cl}}{r_f + t_l + t_g}$
Coolant	$T_{ocl} - T_{bulk} = \frac{q'}{2\pi h_c(r_f + t_l + t_g + t_{cl})} - \frac{q'}{2\pi h_c(r_f + t_l + t_g + t_{cl} + t_{co})}$

The derivation of the fuel section equation began using equation 4.1 and moving the radius, r, out of the denominator and integrating both sides giving equation 4.3.

$$-\frac{r}{2} * q'''(r) = k\frac{dT}{dr} \tag{4.3}$$

After, integrating equation 4.3, it was integrated again giving equation 4.4, which relates the temperature difference between the peak core temperature and the outer temperature of the fuel to the volumetric heat rate, fuel radius, and fuel thermal conductivity.

$$\left(T_{PCT} - T_{of}\right) = \frac{{r_f}^2 q'''(r)}{4k_f} \tag{4.4}$$

In order to simplify equation 4.4, the following relationship was employed, using the linear heat rate (q') instead of the volumetric heat. This relationship is shown in equation 4.5.

$$q'''\pi {r_f}^2 = q' \tag{4.5}$$

After applying equation 4.5, equation 4.6 is derived and can be used to calculate the temperature gradient over the fuel.

$$T_{PCT} - T_{of} = \frac{q'}{4\pi k_f} \tag{4.6}$$

Other sections that utilized conductive heat transfer follow a similar derivation, but must account for the lack of heat generation within the section. In order to account for this, equation 4.1 is rewritten as below.

$$\frac{-1}{r}\frac{d}{dr}\left(kr\frac{dT}{dr}\right) = 0$$

This necessitates the employment of a relationship between heat flux, linear heat rate and Fourier's Law. This relationship, combined with equation 4.1 with no heat generation shown above, is used to set up the equation for integration. This relationship is shown below.

$$\frac{q'}{2\pi r} = q'' = k\frac{dT}{dr} \tag{4.7}$$

$$\int_{r_i}^{r_o} \frac{q'}{2\pi r} dr = \int_{T_i}^{T_o} k dT \tag{4.8}$$

After integrating, the equation for the temperature change in conductive sections with no heat generation is shown below. This equation was utilized for the liner and clad, with the integrated equations being shown in Table 4.4.

$$T_o - T_i = \frac{q'}{2\pi k} * \ln\frac{r_o}{r_i} \tag{4.9}$$

The two convective sections (i.e., gap and coolant) utilized equation 4.2 and involved a much simpler integration. An important part of this integration was understanding where the heat is entering and leaving from the sections. This is shown in Figure 4.1 below as heat is being transported across the gap by convection.

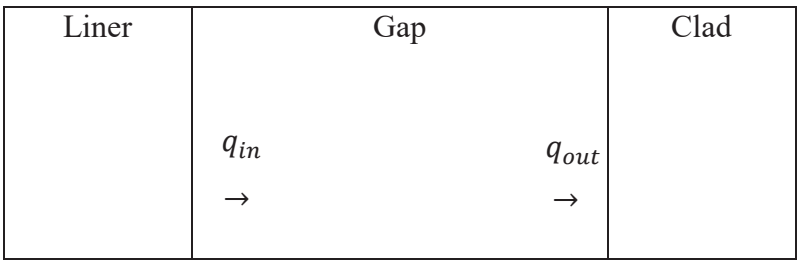

Figure 4.1: Visual Representation of Heat Movement in Gap

Figure 4.1 may seem simple, but it is important to understand that the convective heat transfer equation when solved, only represents the heat transferred through a single surface. In order to derive specific temperature gradients for each fluid section, equation 4.2 is rearranged and solved for the temperature difference as shown in equation 4.10.

$$T_b - T_i = \frac{q'}{2\pi hr} \tag{4.10}$$

Equation 4.2 in this form uses the radius of the surface as r and the heat transfer coefficient of the fluid (h). Equation 4.10 by itself would only be the relationship between the temperature of the surface and the bulk fluid temperature. In order to calculate the temperature at the other surface, this equation is combined with the assumption that heat entering the fluid is positive and heat leaving the fluid is negative. Using this approach, the following equation is created.

$$T_o - T_i = \frac{q'}{2\pi h r_i} - \frac{q'}{2\pi h r_o} \tag{4.11}$$

Equation 4.11 was then used to create the temperature difference equations shown in Table 4.4 for the gap and the coolant. All of the equations listed in Table 4.4 are used to calculate the peak core temperature of the fuel. This is an essential variable to know as it cannot be larger than the maximum allowable temperature. The results of the thermal analyses are included in the next section.

4.2.2 Peak Core Temperature Cases

The results of the thermal analyses are distinguished by the peak core temperature of that case. The UO_2 fueled base case was run at three different temperatures: 1389 K, 1506 K, and 1628 K, which represent reactor power of 1 MWt, 1.5 MWt, and 2.0 MWt or peaking factors of 1.0, 1.5, or 2.0 respectively. These results are shown in Table 4.5 below.

Table 4.5: Uranium Oxide Base Case Thermal Analysis

Temperatures (K)			
Peaking Factor	1.0	1.5	2.0
PCT	1389	1506	1628
Fuel Outer Radius	1207	1235	1264
Liner Outer Radius	N/A	N/A	N/A
Gap Outer Radius	1191	1212	1233
Clad Outer Radius	1190	1209	1230
Bulk Coolant	1150	1150	1150

In order to provide clarity to the locations described in Table 4.5, Figure 4.2 is included below.

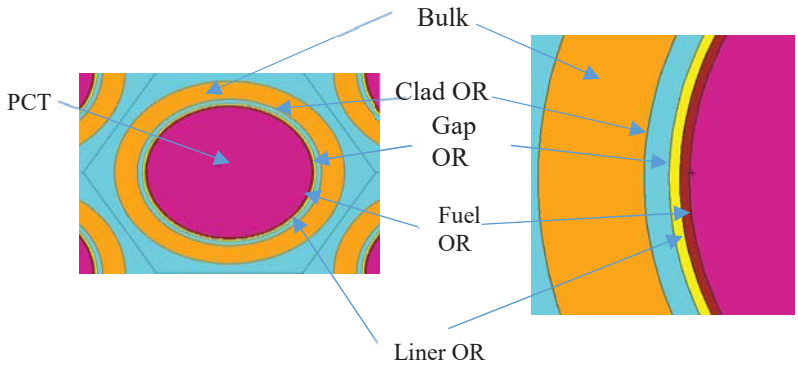

Figure 4.2: Unit Cell Depiction

Figure 4.2 shows how each temperature is related to one another. The base case, which uses UO_2 as fuel, does not need to employ a liner and thus was labeled as non-applicable in Table 4.5 for the temperature of the liner outer radius. This thermal analysis matches the expected outcomes from Project Prometheus, indicating that it was applicable also for the non-oxide fuels.

4.3 Fuel Pin Thermal Expansion

An important aspect of the study was to evaluate how the fuels would react to thermal expansion, which is caused by an increase in temperature within the core. This expansion was calculated using the assumption of a constant mass of material within the core. Thermal expansion results in a change in density of a material. However, each material will expand differently, which also affects the neutron reaction rate and k_{eff}.

For many materials, these temperature-dependent densities are published material properties. However, for the cases where density is not a published material property, the temperature dependent density was calculated. This calculation was done by using the coefficient of thermal expansion (CTE). This was done as shown in equation 4.12, where the ρ' is the material density at temperature T and ρ is the material density at room temperature.

$$\rho' = \frac{\rho}{(1 + CTE * T)^3} \tag{4.12}$$

The derivation of this equation is shown below in equations 4.13-4.19, using a cylinder with original radius r and height h as an example, where the prime over the variable represents the parameter value at temperature T.

$$r' = r + (r * CTE * T) \tag{4.13}$$

$$h' = h + (h * CTE * T) \tag{4.14}$$

$$V = \pi r^2 h \tag{4.15}$$

$$V' = \pi(r')^2 h' = (\pi r^2 h) * (1 + (3 * CTE * T) + (3 * CTE^2 * T^2) + (CTE^3 * T^3)) \tag{4.16}$$

$$V' = \pi(r')^2 h' = (\pi r^2 h) * (1 + CTE * T)^3 \tag{4.17}$$

$$\rho = \frac{m}{V} \tag{4.18}$$

Assuming mass is conserved results in equation 4.12.

$$\rho' = \frac{m}{V'} = \frac{m}{V * (1 + CTE * T)^3} = \frac{\rho}{(1 + CTE * T)^3} \tag{4.19}$$

These calculations were performed for all solid materials in the fuel cell for the three different peak core temperature cases as given in Table 4.5 using a MATLAB code that is included in Appendix B. In order to calculate the temperature dependent densities for the sections containing a gas, a different approach was taken employing the database EasyProp, which gave the temperature dependent density values for helium and the helium xenon mixture [11]. Helium and helium xenon mixture are the gases in the fuel gap and reactor's coolants used in this study as discussed in section 3.1. The values for all temperature dependent densities along with the room temperature (293 K) densities are shown in Table 4.6 below.

Table 4.6: Temperature Dependent Densities of Reactor Materials [7] [2] [11] [12] [13] [14] [15]

Section	Material	Room Temperature Density (g/cc)	CTE (μm/m-(C/K)) All temps in K	Density @ PCT: 1389 K	Density @ PCT: 1506 K	Density @ PCT: 1628 K
Fuel	Uranium Oxide (UO_2)	10.111	13.18 @1600 12.56 @1500 12.01 @1400 In K	9.782	9.739	9.691
Gap	He	0.0033	N/A	0.000801	0.000786	0.000770
Clad	Mo-47.5Re	13.70	6.45 @1273	13.460	13.454	13.449
Block	Mo-47.5Re	13.70	6.45 @1273	13.470	13.470	13.470
Coolant	HeXe	0.0268	N/A	0.00668	0.00668	0.00668
Fission Spring	W-25Re	19.70	5.04 @1273	19.429	19.423	19.417
Axial Reflector	BeO	3.01	7.20 @773	2.954	2.954	2.954

These temperature dependent densities follow as expected, with the higher temperature density being lower than the lower temperature density. This decrease in density results in an increase in reactor volume as the reactor temperature increases.

The temperature dependent densities calculated were then used to calculate the expansion of the different fuel pin sections. The biggest assumption made was that the expansion of the fuel pin was only in the radial direction and no expansion occurred in the axial direction. This assumption was made to reduce the changes required in the MCNP model as the temperature changed. Additionally, the fuel density was modified using equation 4.20 shown below instead of equation 4.12.

$$\rho' = \frac{\rho}{(1 + CTE * T)^2} \tag{4.20}$$

Since axial fuel expansion was not allowed, the full three-dimensional increase in fuel volume would not fit within the gap that exists between the fuel and clad. However, it was felt that this assumption would not significantly affect k_{eff} and to minimize the effect of this assumption, all other non-oxide fuels were evaluated in this manner.

The direction of the expansion of fuel was modeled using orange arrows as seen in Figure 4.3 below where arrows pointing outward signify outward expansion and arrows pointing inward signify inward expansion.

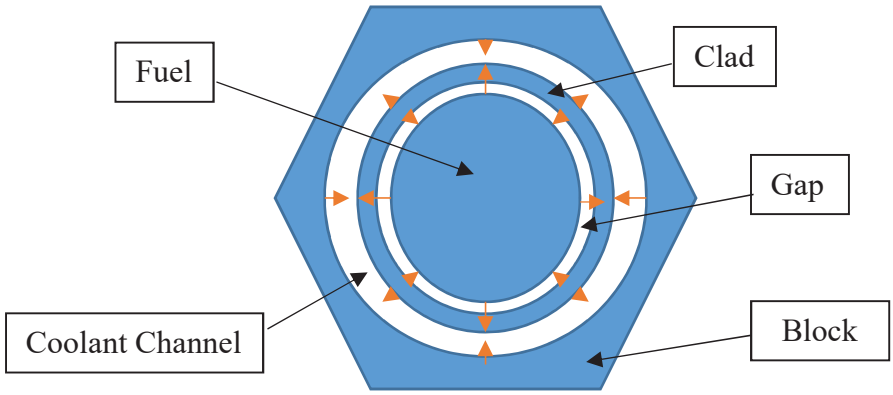

Figure 4.3: Direction of Thermal Expansion in Unit Cell

The fuel was modeled so that all expansion was in the outward direction. The clad was modeled so that 50% of the expansion went inward while 50% of the expansion went outward. Lastly, the block was modeled so that all of the expansion went inwards, to the coolant channel. All expansions were axisymmetric. The methodology started by calculating the volume of the specific section and then calculating the mass of the particular section using density and volume of the section. The mass was then divided by the temperature dependent density giving the volume of the material at that temperature. This volume was then used to calculate the inner and outer radii of the fuel, gap, clad, coolant channel, and block at each of the three peak core temperatures (PCT). The results of this process for each section and peak core temperature in the

unit cell are given in Table 4.7 below. Also given in Table 4.7 are the fuel pin's dimensions at room temperature (293 K).

An addition to Table 4.7 is the spring. The spring is below the fuel in the unit cell and is there to provide support to the fuel during launch, as seen in Figure 3.1(a). Since it must exist within the high temperatures of the core, the spring must be a refractory alloy and thus be accounted for in the thermal expansion analysis.

Table 4.7: Thermal Expansion Parameters of Uranium Oxide Base Case versus Temperature

Section	Characteristic Measurement	Room Temperature (293 K)	PCT: 1389 K	PCT: 1506 K	PCT: 1628 K
Fuel	Fuel Outer Radius (cm)	0.910	0.925	0.927	0.929
Gap	Gap Outer Radius (cm)	0.932	0.931	0.931	0.931
Clad	Clad Outer Radius (cm)	0.983	0.983	0.983	0.983
Coolant Channel	Channel Outer Radius (cm)	1.199	1.193	1.193	1.193
Spring	Spring Outer Radius (cm)	0.737	0.742	0.742	0.743

These temperature dependent inner and outer radii follow the expected expansion shown in Figure 4.3. This change in volume and density is important to include within the neutron transport model as a lower density material is less likely to undergo interactions and thus increase the neutron path length. However, a larger volume allows for more interactions with the material. Thus thermal expansion results in two competing effects on the physics of the core.

4.4 Doppler Broadening

Elevated temperature in core materials also has an impact on neutron interactions. Thermal motion of atoms in each material intensifies with increasing temperature. This phenomenon causes the resonance absorption cross sections to broaden in energy and occurs in nearly all materials. This resonance region is most important in the fuel's isotopes and occurs in uranium isotopes between 1 eV to 1 keV. An example of Doppler broadening's effect on a single low-energy resonance of ^{238}U is shown in Figure 4.4. The vibrational motion associated with higher temperatures affects an absorption cross section resonance in the ^{238}U isotope and widens it over the incident neutron's kinetic energy, but lowers the magnitude of the cross section.

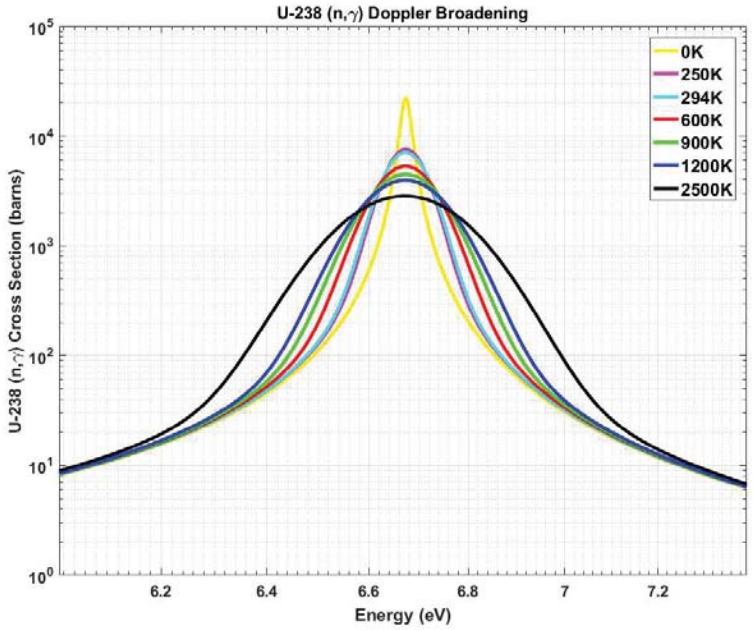

Figure 4.4: Doppler broadening of ^{238}U at 0-2500 K

The area under the curve is independent of temperature, but causes an overall increase in neutron absorption as the temperature increases. Conversely, a decrease in temperature causes a decrease in absorption. This process is important to implement into any code that models

elevated temperatures of fission reactors, especially fast fission reactors due to the large effect of leakage on the compact fast fission reactors. Doppler broadening will cause the resonance absorption to increase with increasing temperature and thus lower the effective multiplication factor of the reactor.

In order to apply Doppler broadening, different cross sections were created using a utility program distributed with MCNP called MAKXSF. This program is used to create the cross sections of the materials at different temperatures. The temperatures created correspond with the values found in the thermal analyses, displayed in Table 4.5. The specifics of how this program is employed are discussed in Appendix C.

4.5 Beginning-of-Life (BOL) Results for UO_2 fueled reactor

The thermal analysis was performed for 100, 150, and 200% power. In each case, the steady state temperature distribution of all materials was found including the PCT of 1389, 1506, and 1628K respectively. Thermal expansion was calculated for each material and the geometric model for MCNP was updated. The temperatures were also used to calculate updated neutron cross sections with MAKXSF. The resulting k_{eff}, accounting for both phenomena was computed using MCNP. These values were compared to room temperature (293 K) to evaluate if the model produced a negative temperature coefficient, which commercial UO_2 fueled reactors are known to have [16].

4.5.1 BOL Effective Multiplication Factor

A plot of k_{eff} is shown in Figure 4.5 below. Each of these cases had a statistical error of approximately 0.00042 and is shown as error bars on the figure. In figure 4.5, keff has been plotted versus the PCT that corresponds to each % power

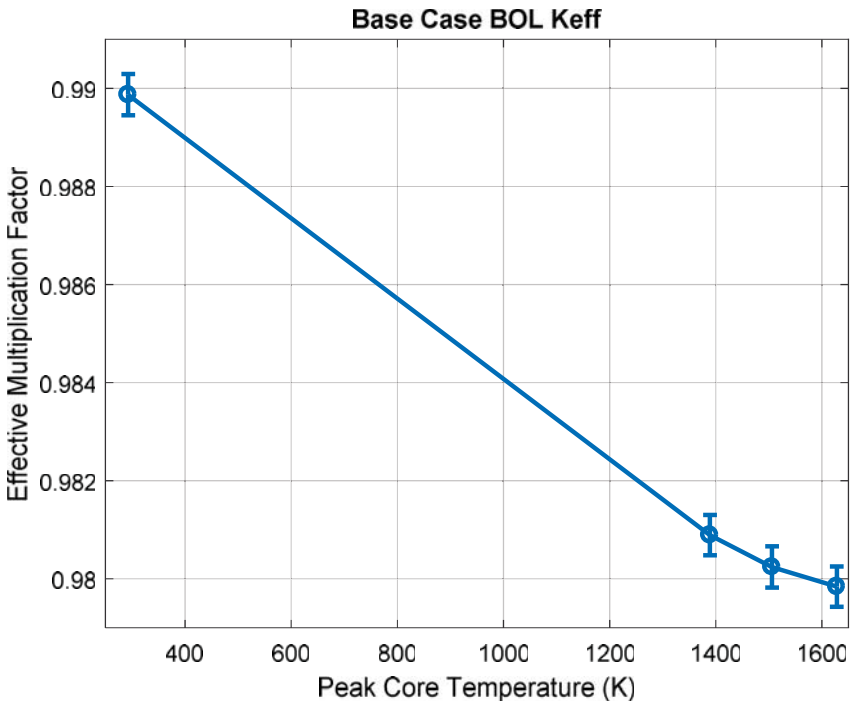

Figure 4.5: Base Case BOL k_{eff} Results

This figure shows that the base case UO_2 is able to stay stable at all temperatures, a concept further discussed in the next section, and matches the expected values for k_{eff}. This is important to note as this demonstrates the likely success of the process for calculating the base case and validates this process for use in the further studies of non-oxide fuels.

4.5.2 BOL Temperature Coefficient of Reactivity

The principal result shown in Figure 4.5 is that k_{eff} decreases as temperature increases. This is indicative of a negative temperature coefficient of reactivity (α_T). The α_T works as a feedback mechanism for the immediate control of the reactor. With a negative α_T, a rise in temperature will add negative reactivity to the core, thus lowering k_{eff} and lowering core power. This change will then cause the temperature to decrease, adding positive reactivity and bringing the core back to the stable power level. Thus, a negative α_T indicates a stable reactor. The α_T is calculated using equation 4.21 below.

$$\alpha_T = \frac{(k_{eff\,2} - k_{eff\,1})}{(T_2 - T_1)} \tag{4.21}$$

Equation 4.21 represents a relationship between two states, an initial and a final state, each with a respective T and k_{eff}. T_1 and $k_{eff\,1}$ represent the initial state with T_2 and $k_{eff\,2}$ representing the final state scenario after a variable has been altered. The α_T is a measure of the slope between the two points in Figure 4.5.

The calculated values of α_T from the BOL base case are included in Table 4.8 below.

Table 4.8: Temperature Coefficient of Reactivity for BOL Base Case

Case	α_T (K^{-1})
293 K→1389 K	-8.193e-6
1389 K→1506 K	-5.556e-6
1506 K→1628 K	-3.279e-6

These α_T values are typical of those representative of a gas cooled reactor which have been reported to be approximately -6e-6/ K [16]. Additionally, α_T is not constant with respect to temperature and thus an equation was generated to model α_T over a range of temperatures (293-1628 K). This equation is included below and utilizes the reactor's temperature, T, to calculate the α_T.

$$\alpha_T(\mathrm{K}^{-1}) = (-3.67e-5) + (2.06e-8) * T(K) \tag{4.22}$$

Equation 4.22 was created using MATLAB to make a linear fit of the values presented in Table 4.8. This code and the code used to produce Figure 4.3 are included in Appendix B.

4.6 Burnup

In order to ensure reactor criticality over its planned lifetime, fuel burnup must be taken into account. Burnup comprises two main phenomena: transmutation and consumption due to

fission of the fuel. Transmutation, as discussed previously, is when an atom of fuel absorbs a neutron and does not fission, instead producing a different isotope. This process is called radiative capture and can lead to the creation of a variety of different isotopes. Some of the isotopes resulting from transmutation will tend to be neutron absorbers; others will undergo fission with high probability. Both effects will manifest as a change in reactivity and thus burnup will change the k_{eff} and the total neutron population within the core.

Fission of fuel atoms leads to a decreasing amount of ^{235}U within the fuel. During the fission reaction, ^{235}U nucleus splits into two different isotopes. The probability of the creation of different fission product isotopes versus their atomic weight is presented in Figure 4.6 below.

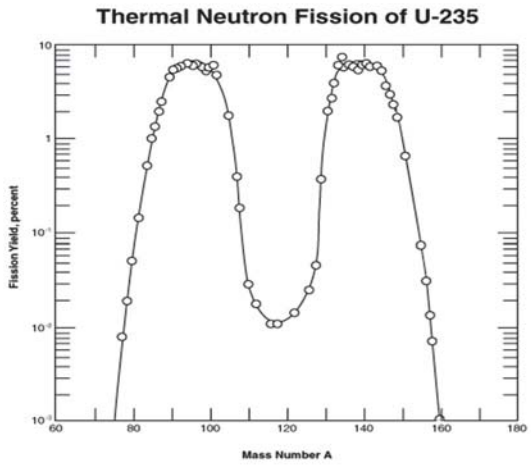

Figure 4.6: Fission Product Yield Curve [17]

This figure relates the atomic mass of the isotope (x axis) to the yield per 100 fissions (y axis). As fission occurs within the reactor, more of ^{235}U will be transformed into the isotopes present in Figure 4.6. Some of these fission products have high neutron absorption cross sections. As these fission products build up, negative reactivity is added thus lowering k_{eff}.

Due to these combined effects, burnup will add negative reactivity, and typically continue to add negative reactivity in larger quantities as lifetime of the fuel increases. In order to keep the reactor critical and the power constant, reactivity needs to be added by movement of the reactor's safety pin or the reflectors.

MCNP has the ability to estimate the combined effects of transmutation, consumption of U-235, and build-up of fission products in burnup calculations. Input parameters for such calculations—including the duration of reactor operation, power level during the time of operation, what materials are included in the burnup process, and what subset of isotopes are to be tracked—are all encoded in an MCNP "burn card". MCNP groups isotopes of interest into "tiers", with increasing tier numbers encompassing larger subsets of nuclides. In this study, the fuel is burned for 15 years at 1 MWt. This analysis also utilizes only tier 1 of available isotopes as isotopes contained in tier 2 or tier 3 would be present in negligible amounts. An explanation of tier number is provided in Appendix D. Further description and discussion of how the burn card was employed is contained within Appendix D.

4.7 MOL Results (7.5 years of operation)

After completing the BOL analysis, a burnup analysis of the Base Case was conducted to evaluate how changes to core composition due to burnup would affect reactor behavior. This analysis tests the reactor's ability to sustain criticality throughout the expected mission time of 15 years. This reactor was analyzed first at MOL (middle of life) which occurs at 7.5 years of operation. The burn card calculation was used to determine the atomic composition of the fuel after 7.5 years of use. These values follow the expected trends that k_{eff} decreases with time.

4.7.1 MOL Effective Multiplication Factor

This analysis was completed using the burn card to calculate the composition of the fuel after 7.5 years of use. In order to accomplish this, the code was run collecting isotopic data at each month.

After adding the appropriate fuel composition, the k_{eff} for room temperature and the three PCTs corresponding to the three power levels (100% , 150%, 200%) was calculated using MCNP and is shown in Figure 4.7 below. The statistical uncertainty for these cases was 0.00042 and the error bars are included in the figure.

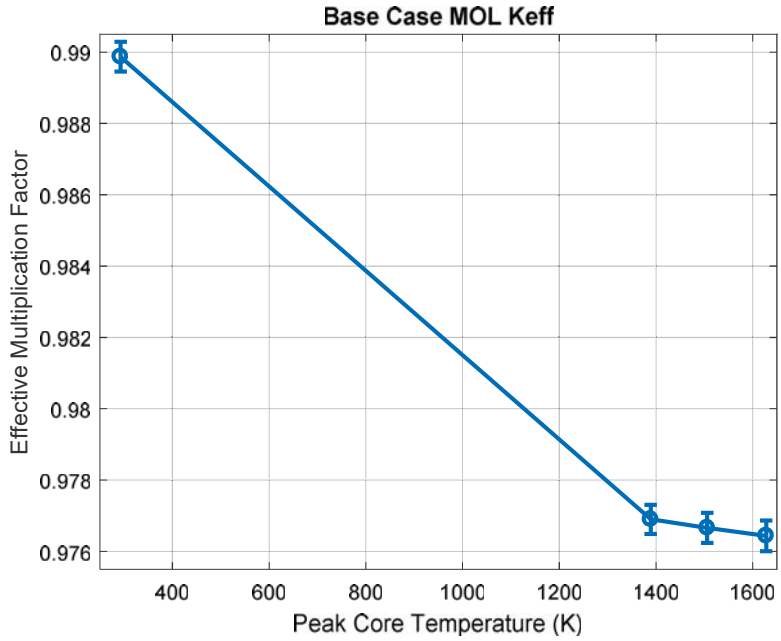

Figure 4.7: Base Case MOL k_{eff} Results

This figure shows that through 7.5 years of life, the reactor can still stay stable at all temperatures and maintain the negative α_T. An important note in Figure 4.7 is that while the values show a negative α_T, the magnitude of this α_T is much smaller than that of BOL. This observation will be discussed in the next section.

4.7.2 MOL Temperature Coefficient of Reactivity and Burnup

As stated in the previous section, the MOL analysis shows that k_{eff} decreases with temperature, indicating a negative α_T. The calculated α_T values for the MOL are shown in Table 4.9 below versus temperature ranges corresponding to the three different reactor powers. These values were calculating using equation 4.21 in section 4.5.2.

Table 4.9: Temperature Coefficient of Reactivity for MOL Base Case

Case	α_T (K^{-1})
293 K→1389 K	-1.183e-5
1389 K→1506 K	-2.051e-6
1506 K→1628 K	-1.803e-6

These α_T values are each significantly less than the α_T values of the BOL case, which is given in Table 4.8. This analysis shows that as the reactor ages, the α_T still remains negative. The equation used to model these values is shown in equation 4.23.

$$\alpha_T(\mathrm{K}^{-1}) = (-6.808e-5) + (4.169e-8) * T(K) \tag{4.23}$$

Fuel burnup is defined as the percentage of the fuel that has fissioned. It was calculated using equation 4.24.

$$burnup\ \% = \frac{0.93 - r}{0.93} * 100\% \tag{4.24}$$

This equation uses r, the enrichment of the fuel at the specific point of life, and 0.93, the original enrichment of the fuel, to calculate the change in enrichment. This value will go up continuously as life of the reactor increases. At MOL, the reactor's enrichment is 0.9225 which gives a burnup of 0.80%.

One possible explanation for the smaller magnitude α_T is the change in density of the fission products. As stated previously in section 4.6, burnup leads to the creation of fission products. Many of these fission products act as poisons and absorb neutrons [4]. However, as temperature increases, the density of these fission products will decrease with the fuel. As the density decreases, the individual atoms become more spread out, lowering the ability of the material to absorb neutrons. This causes the addition of positive reactivity to the core as temperature increases and decreases the α_T.

4.8 EOL Results (15 years of operation)

The EOL analysis follows the same process as MOL, except the data is taken from the reactor after 15 years of simulated use. Section 4.8.1 displays the k_{eff}'s at the different power levels and PCT as used in the MOL analysis, but after 15 years of use. Section 4.8.2 gives the calculation of α_T and the effect of burnup.

4.8.1 EOL Effective Multiplication Factor

This analysis was completed using the same burn card as the MOL analysis. The composition used in this analysis comes from the 180^{th} month created in this burn card. The k_{eff} versus PCT corresponding to the three power levels data is shown in Figure 4.8 below.

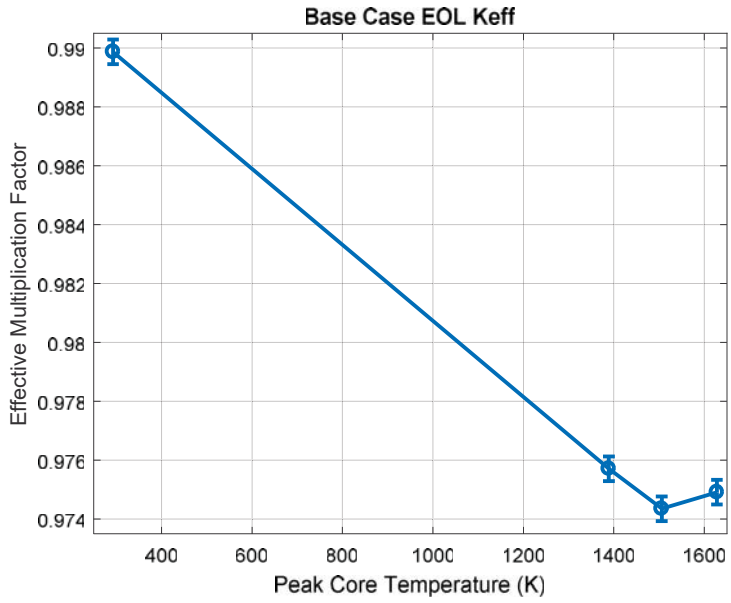

Figure 4.8: Base Case EOL k_{eff} Results

Figure 4.8 begins to show the effect of burnup upon the reactor. This is seen in the increase of k_{eff} between the 150% and 200% power level. The initial change form 100% to 150% power shows a negative α_T, but the following change shows an increase in power. In this case the volume change from 150% to 200% power added more positive reactivity than the negative reactivity added by Doppler broadening.

4.8.2 EOL Temperature Coefficient of Reactivity and Burnup

The α_T's for the EOL case were calculated in the same manner as the BOL and MOL analysis, using Equation 4.21 from Section 4.5.2. These values are shown in Table 4.10 below.

Table 4.10: Temperature Coefficient of Reactivity for EOL Base Case

Case	α_T (K^{-1})
293 K→1389 K	-1.292e-5
1389 K→1506 K	-1.1624e-5
1506 K→1628 K	4.5902e-6

The initial two α_T, from 293 K to 1389 K and 1389 K to 1506 K, follow the expected path, but the change from 150% (1506 K) to 200% (1628 K) power is different and results in a positive α_T. This is addressed by the increase of burnup within the fuel.

The enrichment of the fuel after 15 years is 0.915 compared to the initial enrichment of 0.93. Using equation 4.24, the burnup is 1.613%. As expected, this is roughly twice the burn-up at 7.5 years (0.80%), which results in more fission products being present within the core. As seen in the 150% to 200% power change (1628 K), the positive reactivity added by fission products is larger due to the presence of more fission products. This raises concern regarding the use of UO_2 as a fuel due to its temperature coefficient instability near the end of mission life.

5 Non-Oxide Reactor Development

After completion of the base case model, the next step in the study was to apply the same method of approach to the non-oxide fuels to be studied. The first step in this process was to parametrize the non-oxide reactors. In order to keep the analysis fair and consistent, two things were held constant in the reactor: the mass of uranium and the volume of coolant within the core. This was done as the reactor would use the same average linear power per fuel pin and thus would need to have the same volume and mass flow rate within the core to keep a consistent 1 MWt. One of the expected benefits of non-oxide fuels is the higher loading density, which is expected to allow for a lighter weight reactor. In order to test this, a comparison is made between the mass of the UO_2 fueled reactor and mass of the non-oxide reactors at room temperature. The mass was found for each reactor by calculating the individual volumes of all the reactor components and then multiplying that volume by the specific materials' density at room temperature. In addition to lighter weight and lower volume fuel, the increased loading density allows for a lower volume of other reactor components such as the reactor block and vessel. In order for both reactors to produce the same power, UN and UC fuel outer radius (OR) were chosen to contain the same mass of fuel as in the UO_2 reactor. Now that stronger spectral shift poison are placed within the core, the block and clad material need to be changed to a more average strength spectral shift poison. The material chosen was the niobium and tantalum rich FS-85.

Table 5.1 contains a list of all the reactor components considered in this mass calculation along with dimensions in cm and their density in grams/cm^3. A visual comparison is shown in Figure 5.1

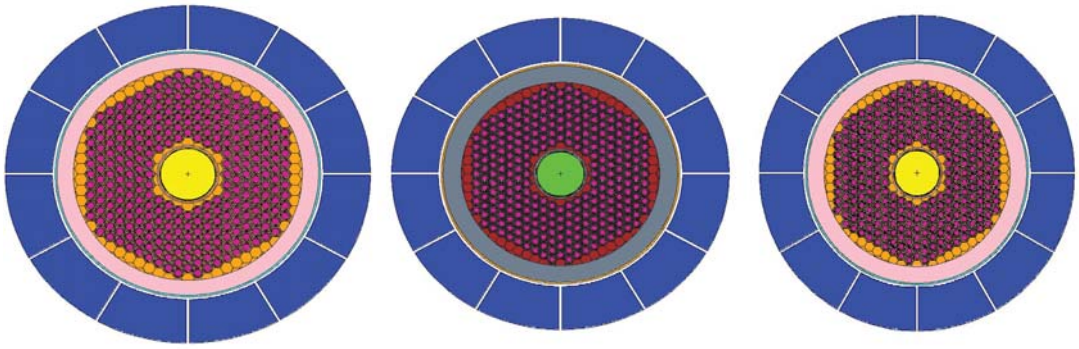

(a) (b) (c)

Figure 5.1: (a) UO_2 Axial View (b) UN Axial View (c) UC Axial View

Table 5.1: Dimensions and Density of UO_2, UN, and UC Reactor Constituents Used in Reactor Mass Comparison

Section	Dimensions (cm)			Density (g/cm^3)		
	UO_2	UN	UC	UO_2	UN	UC
Fuel OR	0.91	0.71	0.73	10.11	14.32	13.63
Liner OR	N/A	0.73	0.75	N/A	21.02	21.02
Gap OR	0.93	0.75	0.77	0.0033	0.0033	0.0033
Clad OR	0.98	0.83	0.82	13.70	10.60	10.60
Coolant Channel OR	1.20	1.06	1.07	0.027	0.027	0.027
Unit Cell OR	1.51	1.32	1.33	13.70	10.60	10.60
Block IR	7.24	6.32	6.40			
Block OR	26.65	23.26	23.54			
Spring OR	0.74	0.58	0.59	19.73	19.73	19.73
Vessel OR	30.91	27.99	28.23	8.50	8.50	8.50
Radial Reflector OR	42.55	39.64	39.88	3.01	3.01	3.01
Safety Pin OR	6.36	5.55	5.62	2.20	2.20	2.20

These masses were calculated using the Mass Comparison MATLAB code contained in Appendix B. This MATLAB code was used, with published density values at room temperature, to calculate the overall weight of separate portions of the reactor as well as the total. The values of this mass comparison are shown in Table 5.2 below.

Table 5.2: Mass Comparison of UO_2, UN, and UC Fueled Reactor

Section	Mass (kg)		
	UO_2	UN	UC
Fuel	651.62	398.11	394.98
Liner	N/A	33.42	34.11
Clad	118.40	74.47	75.90
Block	1025.06	585.15	600.78
Reflectors	528.79	483.06	486.75
Springs	300.75	183.28	191.53
Vessel	140.19	120.56	122.13
Safety Pin Components	81.73	50.32	52.00
Support Structures	252.24	148.74	152.38
Total	3098.78	2077.12	2110.56

Table 5.2 shows that increased loading density allows the mass of fuel in the UN and UC fueled reactors to be significantly lighter than UO_2. In addition, the block and springs masses are nearly 50% less in the UN and UC fueled reactor compared to the UO_2 fueled reactor. The total UN reactor mass was found to be approximately 33% lower than the mass of the UO_2 fueled reactor (3099 kg versus 2077 kg), leading to over a metric ton difference. The total UC reactor mass was found to be approximately 32% lower than the mass of the UO_2, leading to a nearly 988 kg difference in mass. The lower UN and UC reactor mass would be an advantage during space launch due to the need for a smaller booster rocket engine. The UN reactor would still be the best in this regard, as it is the lightest, due primarily to having the highest loading density of the fuels tested.

6 Uranium Nitride

After parametrizing the UN reactor in the previous section, the next step was to analyze the UN reactor with the previously created method of approach. Section 6.1 discusses the use of the method of approach developed during the base case. Section 6.2 discusses the BOL analysis that employed the results of the method of approach into the neutron transport model. Section 6.3 discusses the effect of burnup on the core and the analysis at MOL and EOL.

6.1 Uranium Nitride Method of Approach

The method of approach used in evaluating the UO_2 was repeated for the UN case. The first step in this method was to conduct a thermal analysis similar to the analysis conducted for UO_2. This analysis used the same equations as shown in Table 4.4. The results of this thermal analysis for 100,150 and 200% power are shown in Table 6.1 below. These power levels are represented by the PCT of 1247, 1295, and 1344 respectively.

Table 6.1: UN Thermal Analysis

Temperatures (K)			
PCT	1247	1295	1344
Fuel Outer Radius	1223	1260	1296
Liner Outer Radius	1222	1259	1295
Gap Outer Radius	1214	1246	1278
Clad Outer Radius	1213	1244	1276
Bulk Coolant	1150	1150	1150

An important effect that can be seen in this analysis is the effect of the higher thermal conductivity. The UO_2 fuel saw a temperature gradient between PCT and fuel OR of 182 K for the fuel while the UN has a temperature gradient of just 24 K. In addition to individual fuel temperature gradients, the change from 100% power to 200% power is 97 K for UN. For UO_2,

this same change is 259 K. The smaller temperature change for UN gives it more ability to survive power excursions. Lastly, even at a PF of 2.0, the PCT does not violate the thermal limits of the fuel, 1600 K.

These temperatures are then used first to calculate the thermal expansion of the various points of the core. The results of this thermal expansion analysis are shown in Table 6.2 below.

Table 6.2: UN Temperature Dependent Densities

Section	Material	Room Temperature Density (g/cc)	CTE (μm/m-(C/K)) All temps in K	Density @ PCT: 1247 K	Density @ PCT: 1295 K	Density @ PCT: 1344 K
Fuel	Uranium Nitride (UN)	14.32	8.85 @1247 8.92 @1295 8.99 @1344 In K	14.01	13.99	13.98
Liner	Re	21.02	6.80 @300	20.50	20.49	20.47
Gap	He	0.0033	N/A	0.00079	0.00077	0.00075
Clad	FS-85	10.60	6.45 @1273	10.39	10.38	10.38
Block	FS-85	10.60	6.45 @1273	10.40	10.40	10.40
Coolant	HeXe	0.027	N/A	0.0067	0.0067	0.0067
Spring	W-25Re	19.7	5.04 @1273	19.42	19.41	19.40
Axial Reflector	BeO	3.01	7.20 @773	2.95	2.95	2.95

Table 6.2 shows that due to UN's small change in temperature and low CTE, there is little change in its density at the different power levels and corresponding PCTs. The densities for other core materials was also found to undergo little change with power.

After calculating the temperature dependent densities, these values were used to parametrize the dimensions of the fuel sections at the three different power levels and PCT of the UN reactor. The important dimensions for the various sections for each of these models is shown in Table 6.3 versus PCT

Table 6.3: Thermal Expansion Results for UN

Section	Characteristic Measurement	Room Temperature (293 K)	PCT: 1247 K	PCT: 1295 K	PCT: 1344 K
Fuel	Fuel Outer Radius (cm)	0.7109	0.7178	0.7182	0.7186
Liner	Liner Outer Radius (cm)	0.7309	0.7376	0.7380	0.7383
Gap	Gap Outer Radius (cm)	0.7529	0.7515	0.7515	0.7514
Clad	Clad Outer Radius (cm)	0.8039	0.8035	0.8035	0.8035
Coolant Channel	Channel Outer Radius (cm)	1.0565	1.0500	1.0500	1.0500
Spring	Fuel Outer Radius (cm)	0.5755	0.5796	0.5797	0.5799

Table 6.3 shows again the effect of having smaller temperature changes between different power levels with many of the dimensions undergoing little change.

The last step of the method of approach was to use the temperatures to create more cross sections using MAKXSF; the process for this is shown in Appendix C. These cross sections needed the new temperatures from the UN thermal analysis, as well as the new materials that were used such as niobium and tantalum in the FS-85. After the creation of these cross sections, the method of approach was completed and the analysis of the UN reactor performed.

6.2 Uranium Nitride BOL

The next step in the Uranium Nitride (UN) reactor analysis was to take the values shown in Table 6.3 and 5.1 and apply those to the MCNP neutron transport model. Like the Base Case (UO_2 fueled reactor), this model was run at three levels of power: 100, 150, and 200% power and room temperature. The three power levels are represented by their respective peak core temperature (PCT) values of 1247, 1295, and 1344 K. The k_{eff} of these analyses were compared to the room temperature (293K) k_{eff} in order to determine the temperature coefficient of reactivity for UN reactor at the beginning of core life (BOL).

6.2.1 Uranium Nitride BOL Effective Multiplication Factor

The k_{eff} found is plotted in Figure 6.1 below versus the peak core temperature. The room temperature calculation has a one sigma statistical uncertainty in k_{eff} of +0.00042 while the 100%, 150%, and 200% power levels have an uncertainty of +0.00001 and hence no error bars are provided for these latter cases. The smaller uncertainty in the non-room temperature cases was due to running a much larger number of case histories in the MCNP model.

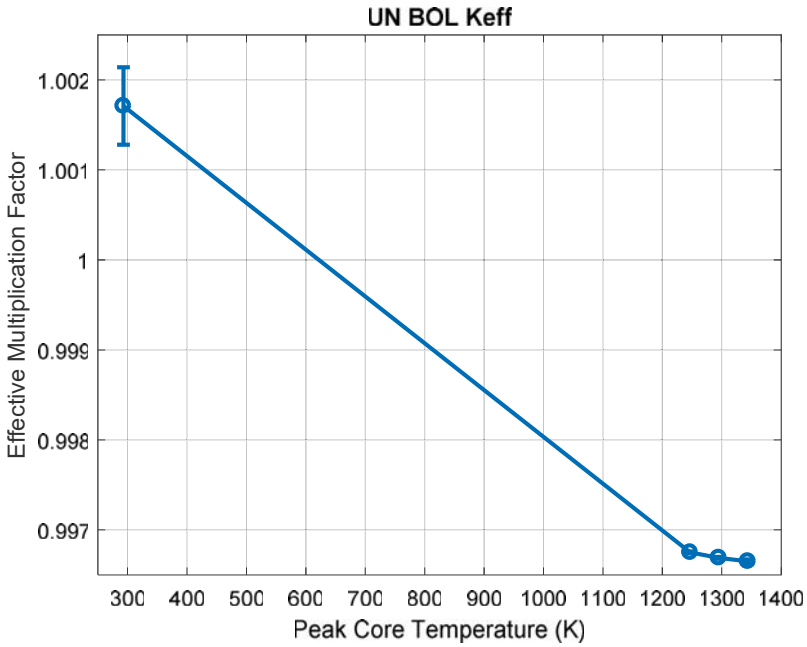

Figure 6.1: Uranium Nitride BOL k_{eff} Versus Peak Core Temperature

This figure shows that UN's k_{eff} decreases with increasing temperature and thus would have a negative α_T. This result indicates that the reactor will likely maintain stability at all expected temperatures of operation at BOL, similar to UO_2.

6.2.2 UN BOL Compared to UO_2 BOL Temperature Coefficient of Reactivity

The difference between the BOL UN and the BOL UO_2 temperature coefficients lie in the magnitude of the negative slope between the temperature increase between 100% power (PCT 1242 K) and 200% power (PCT 1334 K) as shown in Table 6.4. The negative slope between those three values for UN has a lower magnitude indicating that a temperature increase will not add as much negative reactivity for UN compared to a UO_2 reactor. This effect is due to Doppler broadening reactivity for UN being much smaller than for UO_2. The effect is believed to be because the alloying material of the UN reactor, ^{14}N, has a much higher absorption cross section than the alloying material for the UO_2 reactor, ^{16}O [4]. When the UN reactor temperature

increases, the ^{14}N contained in the fuel absorbs fewer neutrons, adding positive reactivity to the core. This positive reactivity from lower density alloying material is larger in the UN reactor than from the O_2 in the UO_2 reactor, which negates some of the effects of the negative Doppler broadening reactivity for the UN reactor. This concept was tested by running trials with the UN reactor, using fuel that was 50% ^{14}N and 50% ^{15}N and then 100% ^{15}N versus it being all ^{14}N. ^{15}N has a much smaller cross section than ^{14}N and would have more similar neutron absorption characteristics to O_2. The results of these trials are shown in Table 6.4. These results show that with the addition of ^{15}N, with its lower cross section, the temperature coefficient becomes more negative as expected.

The α_T 's for all UN cases are calculated using equation 4.21 from section 4.5.2. The values of these calculations are shown in Table 6.4 below compared to the α_T for UO_2.

Table 6.4: Temperature Coefficient of Reactivity for BOL UN and UO_2

Case	UN α_T (K^{-1})			UO_2 α_T (K^{-1})
	100% N-14	50% N-14/50% N-15	100% N-15	
RT→100% Power	-5.199e-6	-3.082e-6	-3.270e-6	-8.193e-06
100→150% Power	-1.250e-6	-2.083e-6	-3.333e-6	-5.556e-06
150→200% Power	-8.163e-7	-1.225e-6	2.449e-6	-3.279e-06

These values are in some cases much different from the expected α_T for a UO_2 fueled gas cooled reactor (-6e-6). Similar to the base case analysis, these values were used to generate an equation for calculating α_T between these temperatures (293-1344 K), which is given by equation 6.1 below.

$$\alpha_T(\mathrm{K}^{-1}) = (-6.08e-5) + (4.51e-8) * T(K) \quad (6.1)$$

6.3 Uranium Nitride Burnup

After completing the BOL analysis for UN, the next step was to conduct the burnup analysis and measure the k_{eff} for MOL. This was done in the same fashion as the UO_2 burnup, with the k_{eff} being measured at each month through the 15-year lifetime. Figure 6.2 below shows the k_{eff} of each power level and corresponding PCT with the fission product composition associated with 7.5 years of use at an average power level.

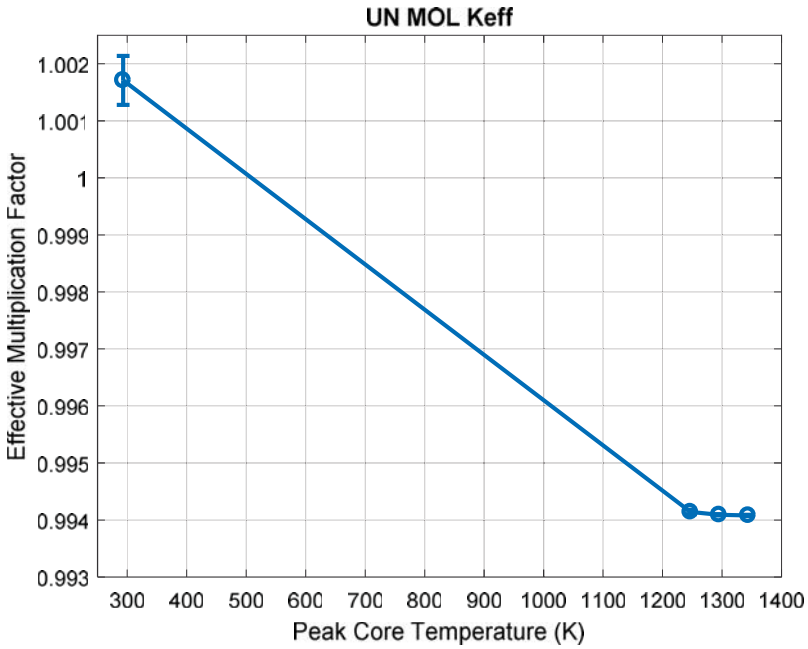

Figure 6.2: UN Middle of Life k_{eff}

As seen in Figure 6.2, the α_T at all changes in power level is negative indicating a negative α_T. The values of the α_T for the various temperature ranges corresponding to reactor power is shown in Table 6.5 below.

Table 6.5: UN MOL Temperature Coefficient of Reactivity

Case	α_T (K^{-1})
293 K→1247 K	-7.935e-6
1247 K→1295 K	-1.042e-6
1295 K→1344 K	-2.041e-7

Table 6.5 shows that the UN reactor will be able to maintain an adequate level of safety at the 7.5 year point. In addition, using equation 4.21 in section 4.7.2, the burnup was calculated to be 0.817% at MOL which is slightly more than the burnup of 0.806% that UO_2 experiences at the MOL mark. This larger burnup is due to the higher percentage of uranium in the fuel.

The final step in analyzing the UN was the EOL analysis. This was done to see if it could maintain safety after its 15 year mission. The k_{eff} of each power level are plotted below in Figure 6.3 versus PCT.

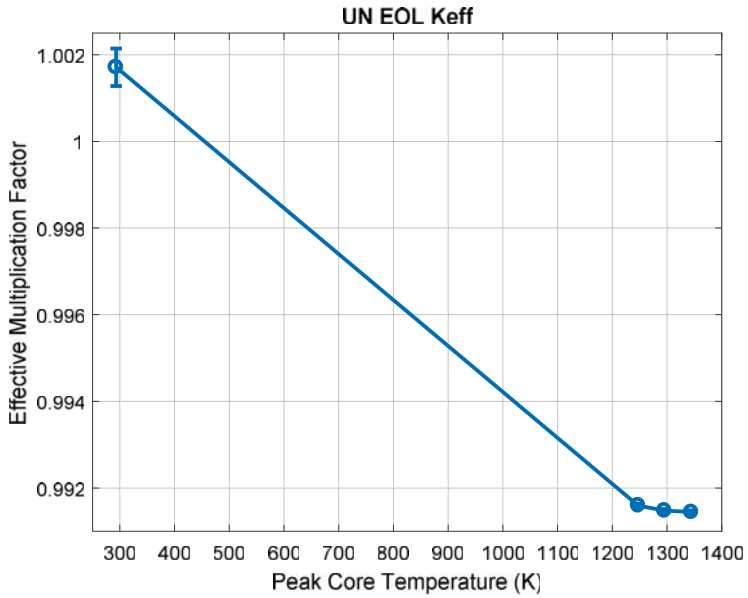

Figure 6.3: UN End of Life k_{eff}

Figure 6.3 shows that the UN reactor is able to maintain a negative α_T throughout the entirety of its 15 year lifetime. The specific α_T values of each transition is shown in Table 6.6 below versus specific temperature ranges corresponding to changes in reactor power.

Table 6.6: UN EOL Temperature Coefficient of Reactivity

Case	α_T (K^{-1})
293 K→1247 K	-1.060e-5
1247 K→1295 K	-2.500e-6
1295 K→1344 K	-6.122e-7

As stated above and seen in Table 6.3, UN is able to maintain a negative α_T throughout its lifetime. The burnup of the reactor at EOL was 1.634% which was slightly more than the 1.613% that UO_2 experiences at EOL. This means that UN is able to maintain adequate safety while also operating with a significantly lower reactor mass than UO_2.

7 Uranium Carbide

After completing the UN analysis, the next step was to analyze the UC reactor with the previously created method of approach. Section 7.1 discussed the use of the method of approach developed during the base case. Section 7.2 discusses the BOL analysis. Section 7.3 discusses the effect of burnup on the core and the analysis at MOL and EOL.

7.1 Uranium Carbide Method of Approach

The method of approach used in evaluating the UO_2 was repeated for the UC case. The first step in this method was to conduct a thermal analysis similar to the analysis conducted for UO_2. This analysis used the same equations as shown in Table 4.4. The results of this thermal analysis for 100,150 and 200% power are shown in Table 7.1 below. These power levels are represented by the PCT of 1242, 1288, and 1334 respectively.

Table 7.1: UC Thermal Analysis

Temperatures (K)			
PCT	1242	1288	1334
Fuel Outer Radius	1220	1255	1290
Liner Outer Radius	1219	1254	1289
Gap Outer Radius	1212	1242	1273
Clad Outer Radius	1210	1241	1271
Bulk Coolant	1150	1150	1150

An important effect that can be seen in this analysis is the effect of the highest thermal conductivity among evaluated fuels. The UO_2 fuel saw a temperature gradient of 189 K between the PCT and fuel OR for the fuel while the UC has a temperature gradient of just 22 K. In addition to individual fuel temperature gradients, the change from 100% power to 200% power is 92 K for UC. For UO_2, this same change is about 259 K. The smaller temperature change for UC

gives it more ability to not violate thermal limits of the fuel. Lastly, even at a PF of 2.0, the PCT does not violate the thermal limits of the fuel, 1600 K.

These temperatures in Table 7.1 are then used first to calculate the thermal expansion of the various sections of the core. The results of this thermal expansion are shown in Table 7.2 below.

Table 7.2: UC Temperature Dependent Densities

Section	Material	Room Temperature Density (g/cc)	CTE (μm/m-(C/K)) All temps in K	Density @ PCT: 1242 K	Density @ PCT: 1288 K	Density @ PCT: 1334 K
Fuel	Uranium Carbide (UC)	13.63	10.1 @All T	13.36	13.35	13.34
Liner	Re	21.02	6.8 @300	20.51	20.49	20.47
Gap	He	0.0033	N/A	0.00079	0.00077	0.00076
Clad	FS-85	10.60	6.45 @1273	10.390	10.38	10.38
Block	FS-85	10.60	6.45 @1273	10.40	10.40	10.40
Coolant	HeXe	0.027	N/A	0.0067	0.0067	0.0067
Spring	W-25Re	19.7	5.04 @1273	19.42	19.41	19.41
Axial Reflector	BeO	3.01	7.20 @773	2.95	2.95	2.95

Table 7.2 shows that even though UC has a lower PCT then UN, its density is still going to change more due to the higher CTE of UC.

After calculating the temperature dependent densities, these values were used to calculate section dimensions for the different power levels and PCT of the UC reactor. The important dimensions for each of these cases is shown in Table 7.3.

Table 7.3: Thermal Expansion Results for UC

Section	Characteristic Measurement	Room Temperature (293 K)	PCT: 1242 K	PCT: 1288 K	PCT: 1334 K
Fuel	Fuel Outer Radius (cm)	0.7258	0.7329	0.7332	0.7336
Liner	Liner Outer Radius (cm)	0.7458	0.7527	0.7530	0.7534
Gap	Gap Outer Radius (cm)	0.7678	0.7673	0.7673	0.7673
Clad	Clad Outer Radius (cm)	0.8188	0.8193	0.8193	0.8193
Coolant Channel	Channel Outer Radius (cm)	1.0687	1.0631	1.0631	1.0631
Spring	Spring Outer Radius (cm)	0.5883	0.5925	0.5926	0.5927

Table 7.3 shows again the effect of having smaller temperature changes between different power levels with much of the dimensions not changing significantly.

The last step of the method of approach was to use the temperatures to create more cross sections using MAKXSF. These cross sections needed the new temperatures from the UC thermal analysis, as well as the new materials that were used such as carbon mixture used in the fuel. After the creation of these cross sections, the method of approach was completed and the analysis of the UC reactor performed.

7.2 Uranium Carbide BOL

The next step in the UC analysis was to take the values shown in Table 7.3 and Table 5.1 and apply those to the MCNP neutron transport model. Like the Base Case, this model was run at

three levels of power: 100, 150, and 200% power and room temperature Theses three power levels are represented by their respective peak core temperature (PCT) values of 1242, 1288, and 1334 K. The k_{eff} of these analyses were compared to the room temperature (293K) k_{eff} in order to determine the temperature coefficient of reactivity for UC.

7.2.1 Uranium Carbide BOL Effective Multiplication Factor

The k_{eff} found are plotted in Figure 7.1 below versus the peak core temperature. The room temperature calculation has a one sigma statistical uncertainty in k_{eff} of +0.00042 while the 100%, 150%, and 200% power levels have an uncertainty of +0.00001 and hence no error bars are provided for these latter cases. The smaller uncertainty in the non-room temperature cases was due to running a much larger number of case histories in the MCNP model.

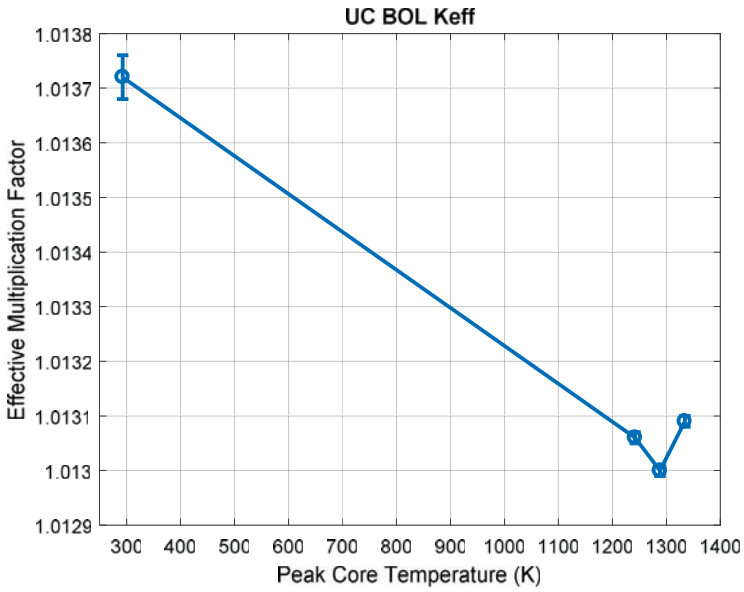

Figure 7.1: Uranium Carbide BOL k_{eff} Versus Peak Core Temperature

This figure shows that UC's k_{eff} decreases with increasing temperature until the 150% power level (PCT 1288 K). This means the fuel is stable until the increase in power from 150 to 200% power (PCT 1334 K). At this point, the k_{eff} becomes positive indicating any increase in

temperature will cause positive reactivity to be added to the core instead of negative. This can lead to the thermal limits of the fuel being violated.

7.2.2 UC BOL Compared to UO_2 BOL Temperature Coefficient of Reactivity

As stated in the previous section, the α_T for UC is negative until 150% power mark and positive after that point. This indicates that if an excursion were to occur that caused a spike in power beyond this point, the reactor will likely become unstable. The fuel would require other control methods to maintain safety.

The α_T for UC is calculated using equation 4.21 from section 4.5.2. The values of these calculations are shown in Table 7.4 below compared to the α_T for UO_2.

Table 7.4: Temperature Coefficient of Reactivity for BOL UC and UO_2

Case	UC α_T (K^{-1})	UO_2 α_T (K^{-1})
RT→100% Power	-5.585e-7	-8.193e-06
100→150% Power	-1.304e-6	-5.556e-06
150→150% Power	1.957e-7	-3.279e-06

In addition to having a positive α_T over the upper temperature ranges, the magnitude of the α_T is also smaller than UO_2. This is believed to be due to the carbon within the fuel. Unlike ^{14}N and ^{16}O, carbon does not absorb a significant fraction of neutrons; its absorption cross section is two orders of magnitude smaller than ^{14}N or ^{16}O [4]. However, because of its lower mass, carbon does serve as an effective neutron moderator with the capability of thermalizing neutrons to lower energy levels. Due to this effect, it is believed that the alloying material of carbon is moderating the neutrons to a thermal level where they are much more likely to cause fission and add positive reactivity to the reactor.

7.3 Uranium Carbide Burnup

After completing the BOL analysis, the burnup analysis was conducted for UC. The k_{eff} for all the MOL cases is shown plotted below on Figure 7.2 versus PCT.

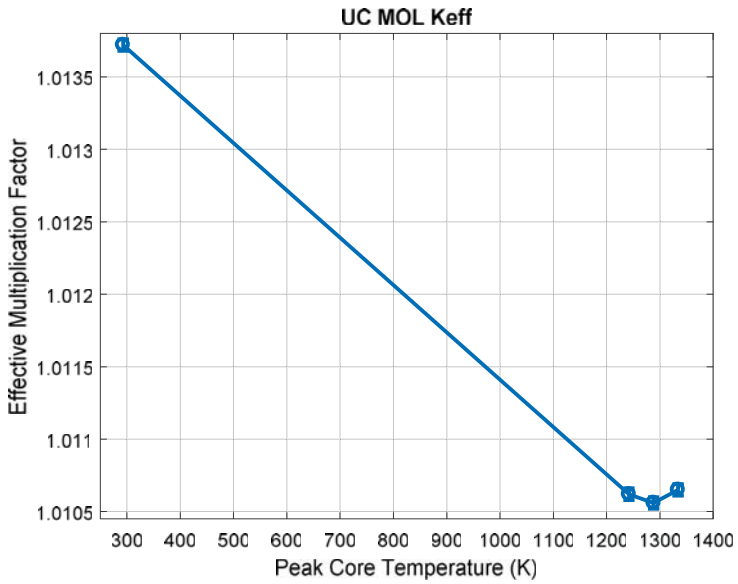

Figure 7.2: UC Middle of Life k_{eff}

Figure 7.2 shows that over core life, the general trend for the behavior of α_T persists. The fuel still exhibits a positive α_T between the 150 and 200 percent power levels (1288 K→1334 K). The values of the α_T are shown in Table 7.5 below versus temperature ranges that corresponds to the different power levels.

Table 7.5: UC MOL Temperature Coefficient of Reactivity

Case	α_T (K^{-1})
293 K→1242 K	-3.267e-6
1242 K→1288 K	-1.304e-6
1288 K→1334 K	1.957e-6

Table 7.5 shows that UC has much smaller feedback due to temperature. This is believed to be due to the neutron absorbing fission products nullifying the positive reactivity being added by the carbon within the fuel. The burnup was calculated to be the same as the UN case (0.817%) as there was the same amount of ^{235}U present within the core.

The final step in the UC analysis was to analyze the reactor at EOL with the full amount of fission products present within the core. The k_{eff} for each power level are shown in Figure 7.3 below versus PCT.

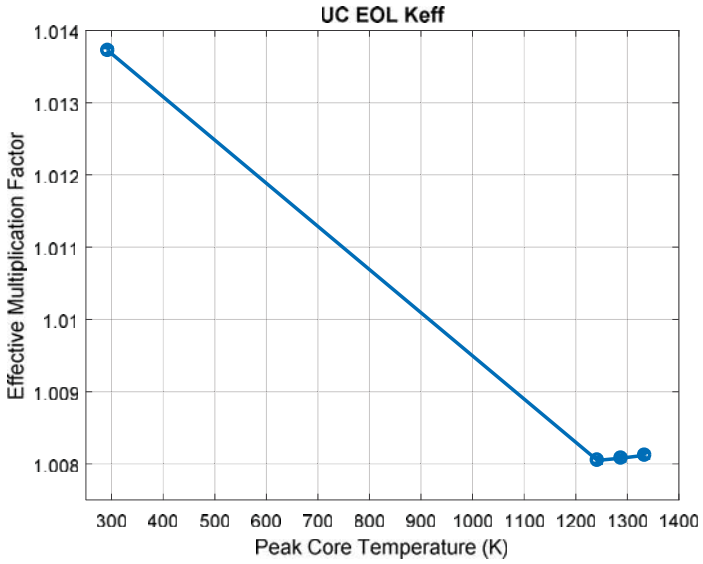

Figure 7.3: UC End of Life k_{eff}

Figure 7.3 shows that the α_T is positive after the 100% (1242 K) power level and maintains the positive level through to the 200% level (1334 K). The values of the α_T are shown in Table 7.6 below versus temperatures that correspond to reactor power levels.

Table 7.6: UC EOL Temperature Coefficient of Reactivity

Case	α_T (K^{-1})
293 K→1242 K	-5.975e-6
1242 K→1288 K	6.522e-7
1288 K→1334 K	8.696e-7

Table 7.6 shows that the additional burnup causes even the 100-150% (1242 K→1288 K) power change to have a positive α_T. This effect is believed to be caused by the presence of greater concentration of neutron-absorbing fission product isotopes in the fuel material. Under these conditions, increased temperature and the associated thermal expansion of the fuel reduces the atom-density of these fission products thus adding positive reactivity to the core.

8 Uranium Molybdenum

Uranium Molybdenum was one of the original candidates for use within the fuel and appeared very promising as it had the largest loading density (16.9 gU/cc) and highest thermal conductivity (0.272 W/cmK) of all candidate materials considered for this study. It was initially understood that UMo would have more restrictive thermal limits due to it being a metallic fuel. It was further determined that UMo would exhibit unacceptable dimensional instability due to accumulation of fission product gasses over core life. Consideration of both of these effects indicates that UMo may be unsuitable for the intended application of this reactor. Section 8.1 discusses the further issues with UMo's lower thermal limits. Section 8.2 will further discuss the effect temperature has on UMo's gaseous swelling.

8.1 Thermal Properties

Initial estimates showed the maximum allowable temperature of UMo to be approximately 750 K. Above this temperature, the fuel begins to dissociate the uranium and the molybdenum causing significant degradation that may ultimately lead to fuel failure. Furthermore, studies into the Reduced Enrichment for Research and Test Reactors (RERTR) experiments have shown that UMo may suffer degradation due to phase dissociation during prolonged operation at temperatures at or below 750 K. Figure 8.1, shown below, is the time-temperature-transformation diagram of UMo [8]. This diagram shows how long a certain composition of UMo can survive at higher temperature before it will begin the phase dissociation. The composition of UMo that was intended for use within the reactor is U-10Mo, which has 10-wt% molybdenum. This plot uses (at%), which is what percentage of the atoms that are a particular isotope. 10-wt% molybdenum is equal to 18-at% molybdenum.

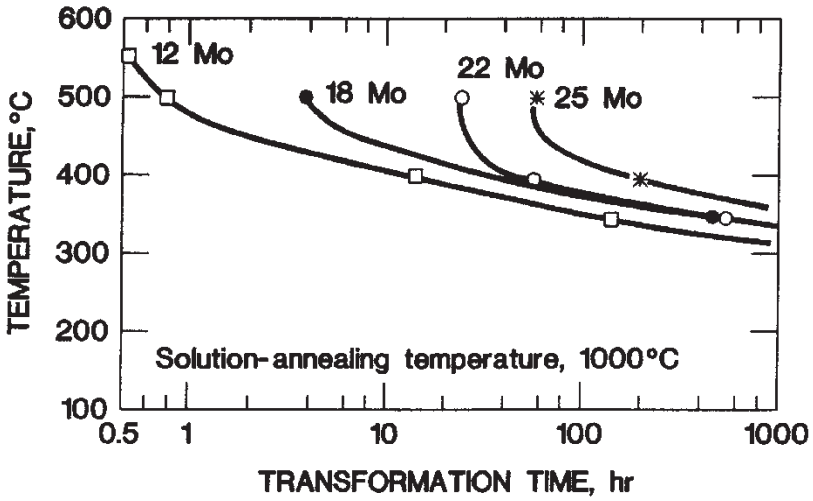

Figure 8.1: TTT Diagram for Uranium Molybdenum (at%) [8]

Figure 8.1 shows that the U-18 Mo fuel can only exist at 750 K for approximately 8-10 hours before it dissociates. The expected duration of this mission is 15 years which translates to 100,000 hours. This time period is not covered on this plot, but using this plot to estimate means the fuel could have a temperature no higher than 350 C. Lowering the temperature of the fuel, simultaneously lowering the temperature of the coolant, will have a large negative effect on the thermal efficiency of the secondary portion of the reactor. This inefficiency may negate the benefits of lowered mass of the primary side of the reactor.

8.2 Gaseous Swelling

In addition to having restrictive maximum temperature limitations, UMo also exhibits dimensional instability—swelling—due to accumulation of gasses during burnup [8]. Several fission products of ^{235}U are created in the gas state. The metallic structure of UMo does not provide an effective path to release these fission product gasses. Due to this inability, fission product gasses build up over core life, the fuel will begin to swell. Figure 8.2 shows the effect temperature has on the fission gas swelling of various compositions of UMo by plotting %

increase in fuel volume versus operating temperature. UMo composition given in this figure is the weight percent.

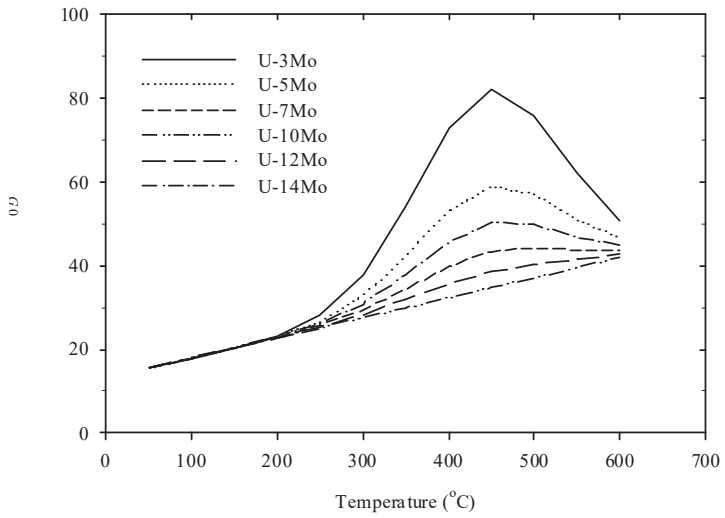

Figure 8.2: Gaseous Swelling due to Temperature in Uranium Molybdenum [8]

Figure 8.2 shows that UMo will exhibit a volume change of 25-40% due to gaseous swelling at temperatures as low as 200-300 °C during operation. Volumetric changes of this magnitude were deemed unacceptable and likely to negate any potential benefits of the metallic fuel.

These two attributes do not mean that UMo is an ineffective fuel for all applications. It was one of the original choices as it is the fuel to be used for the Kilopower space project and is being developed by Y12 now [1]. However, Kilopower is able to do this as it experiences very little burnup over its expected lifetime and there will be very little fission gas created to induce the swelling.

9 Conclusions

After completing the analysis of all the non-oxide fuels, the most important conclusion is that the UN and UC non-oxide fuels may be promising for use as a fuel for a fast compact reactor for space applications. This analysis indicates that, owing to higher fuel loading density, a core employing UC or UN fuel could be both smaller and lighter than a core with UO_2-based fuel with the same power output and same core life.

Our results indicate that UN has significant advantages. The higher uranium loading density of UN fuel results in a reactor that is 33% lighter than the UO_2 base case. This results in an estimated weight savings for the reactor of over 1000 kg. In addition to a smaller and lighter core, UN is able to maintain a negative α_T throughout lifetime; this attribute provides a stabilizing feedback mechanism to reactor power thereby enhancing operational safety. The study results indicate, however, that the magnitude of α_T is generally lower than UO_2-based fuels; an effect that this study attributes to the relatively high neutron absorption cross section of the isotope ^{14}N.

The high uranium loading density achievable with UC fuel also allows for a smaller and lighter core than what can be accomplished with UO_2 fuel. However, this study shows that a core loaded with UC fuel may not maintain a negative α_T throughout core life. For this reason, further studies are warranted to develop alternative reactivity feedback mechanisms that would allow stable and controllable power operation for a core with UC fuel.

UMo appeared to be an excellent choice due to its high loading density and thermal conductivity as well as its promising performance in a current reactor designed for space operation: Kilopower. However, Kilopower is only capable of using it as a fuel due to the much lower burnup expected compared to the burnup in this project [18]. As burnup increases,

significant fuel swelling occurs, an effect that increases with temperature. To overcome this problem, a much larger reactor would be needed. In addition, the thermal limits of UMo are such that it would be impossible to sustain any high temperature operation for an extended period, which would reduce the thermodynamic efficiency of the propulsion plant.

10 Future Work

This project could be further continued in many ways. The first step in continuing it would be to discretize the fuel and other sections of the fuel pin and block so that an axial variation of the fuel temperature could be employed. This would allow for a more accurate thermal analysis and could model the effects of the temperature more accurately on neutron interactions in the core. This could be done with a simple addition of an axial sinusoidal temperature distribution and further refined by including a radial temperature distribution across the core.

The neutron flux distribution could be determined spatially in the axial and radial directions. Such an analysis would provide insight into the relative importance of spectral shift poisons in various reactor materials. These poisons, being refractory alloys, tend to be significantly heavy and elimination of them would allow for even more weight savings.

In addition to a more robust thermal analysis, a more thorough analysis of the control methods of the reactor dynamics such as movement of the reflectors or removal of the safety pin should be analyzed. This transient analysis could prove beneficial in supporting use of the non-oxide fuels that are not as easily controlled by temperature due to having a small magnitude or negative α_T during the reactor lifetime.

Other future work includes a radiological analysis that studies and test the effects of irradiating the material within the core. This will impact the fuel's thermal conductivity and swelling and likely change the geometry of the reactor. Part of this step would be to perform the actual irradiation testing within an advanced test reactor, as much of this irradiation testing has not been completed on the non-oxide fuels.

In addition to all this, more fuels could be tested such as U-Zr-H fuel. Other fuel types such as cermets, ceramic bonded to a metal, have proven to be ideal in the conditions of a fast reactor. Testing these fuels would require significant work as it would completely change the geometry of the core. Other fuels that could be tested include enriching the UN fuel with ^{15}N in order to increase the magnitude of the α_T. UN fuel enriched with ^{15}N would cause more negative reactivity feedback to occur with changes in temperature, possibly increasing safety of the reactor.

Another important future work step to determining the effectiveness of the reactor as a whole would be to perform a balance of plant analysis on the combined primary and secondary systems. This analysis would yield the thermal efficiency and total system weight. This is important to the overall study, as this would indicate the effectiveness of the fuel in creating the electric power needed for operation rather than just thermal power.

The last future work that could be applied to this study is a system structural analysis. This analysis would test the effect a launch or landing due to vibrations on the core components. Additionally, an accident analysis could be performed that studied the consequences of a system explosion during launch or crash on earth. This would be done in order to test if the spacecraft would be able to survive an impact and keep all the radioactive components contained. Proving the ability to contain all radioactive components or only releasing a minimal amount would strengthen the argument for conducting this mission.

11 References

[1] P. Mcclure and R. Robinson, "Nuclear Systems Kilopower Overview," NASA, Cleveland, OH, 2016.

[2] M. Wollman and M. Zika, "Prometheus Project Reactor Module Final Report," Knolls Atomic Power Laboratory, Bettis Atomic Power Laboratory, 2006.

[3] J. C. King and M. S. El-Genk, "Submersion criticality safety of fast spectrum space reactors: Potential spectral shift absorbers," Elsevier, 2005.

[4] J. Kopecky, "Atlas of Neutron Capture Cross Sections," International Nuclear Data Committee, Vienna, 1997.

[5] Haynes International, "Haynes 230 Alloy," 2017.

[6] R. W. Buckman, M. Kangilaski and P. A. Ring, "The production of ASTAR-811C Ingot, Plate and Sheet," American Institute of Physics, 1992.

[7] W. Ranken, "Irradiation Effects on Fuels for Space Reactors LA-UR-84-2651," Los Alamos National Laboratory, Los Alamos, 1986 .

[8] Y. K. J. Rest, "U-Mo Fuels Handbook Version 1.0," Argonne National Laboratory and Idaho National Laboratory, 2006.

[9] "Guide to Engineered Materials Vol. 156," 1999.

[10] R. A. Knief, Nuclear Engineering: Theory and Technology of Commercial Nuclear Power, Albuquerque, NM: American Nuclear Society, 2014.

[11] I. H. Bell, J. Wronski, S. Quoilin and V. Lemort, "Pure and Pseudo-pure Fluid Thermophysical Property Evaluation and the Open-Source Thermophysical Property Library CoolProp," *Industrial & Engineering Chemistry Research,* vol. 53, no. 6, pp. 2498-2508, 2014.

[12] IAEA, "Thermophysical properties database of materials for light water reactors and heavy water reactors," IAEA, Vienna, 2006.

[13] Rhenium Alloys, "Mo-47.5Re Molybdenum-Rheniu Alloy, Annealed Mechanical and Physical Properties".

[14] "MatWeb," [Online]. Available: http://www.matweb.com/search/datasheet.aspx?matguid=ec5e2badc6cf467191fd545182b139ef&ckck=1. [Accessed September 2016].

[15] "Matweb," [Online]. Available: http://www.matweb.com/search/DataSheet.aspx?MatGUID=5951e3aa6454483abb2d04ae896155b6. [Accessed September 2016].

[16] J. J. Duderstadt and L. J. Hamilton, Nuclear Reactor Analysis, Wiley, 1976.

[17] R. W. Mills, "Fission product yield evaluation," University of Birminghan, Birmingham, AL, 1995.

[18] M. A. Gibson, S. R. Oleson, D. I. Poston and P. McClure, "NASA's Kilopower Reactor Development and the Path to Higher Power Missions," NASA Glenn Research Center, Cleveland, 2017.

[19] F. B. Brown, "The maksxf Code with Doppler Broadening," Los Alamos National Laboratory, Los Alamos, NM, 2006.

[20] Los Alamos National Laboratory, "MCNP6 User's Manual," Los Alamos National Laboratory, Los Alamos, NM, 2013.

[21] N. Andrews, "Primary Calculation of the Linear Heat Rate Generation of a BWR Pin in the ATR B-11 Position," State College, PA, 2010.

Appendix A: MCNP Codes

Example BOL Base Case MCNP Model

```
Basic UO2 Reactor (Base Case, pg 55 of B-SE-0155_Reactor_FinalReport)
c
34567891123456789212345678931234567894123456789512345678961234567897123456789 8
c ************************************
c run on 18OCT17 2000 runs and most recent density values
c This run includes all density and volume value changes
c This includes corrected cross sections
c 1389K PCT
c ************************************
c
c Cells
c
c Vessel
10 5 -8.498 -100  101 -102 103          imp:n=1 $ OV Cylinder Portion
11 5 -8.498 -104  105  102              imp:n=1 $ Outer Vessel Upper Dome
12 5 -8.498 -106  107 -103 605.1        imp:n=1 $ Outer Vessel Lower Dome
13 5 -8.498 -109  108                   imp:n=1 $ Vessel Skirt
14 0       -108  104                   imp:n=1 $ Interior of Vessel Skirt
15 0       -110  100  104 106   109 900
          #70 #71 #72 #73 #74 #75 #76
          #77 #78 #79 #80 #81 #82      imp:n=1 $ Space Surrounding Craft
16 0       -110 -100  106 900.3        imp:n=1 $ Space Surrounding Craft
17 0       -110 -100 -201 106   605     imp:n=1 $ Space Surrounding Craft
18 0        110                        imp:n=0 $ Void outside of 14
c
c Inner Core Structures
20 5  -8.498     200  205   -204     imp:n=1 $ Inner Dome
21 71 -0.00668  -203  605.1 -200 201 imp:n=1 $ Coolant Up-Comer
22 71 -0.00668  -101  202   -305 309 imp:n=1 $ Coolant Down-Comer
23 71 -0.00668  -105  204    200     imp:n=1 $ Coolant B/t Inner and Outer Dome
24 71 -0.00668  -205  200            imp:n=1 $ Coolant In Inner Dome
25 71 -0.00668  -107  605.1 -201     imp:n=1 $ Coolant In Lower Dome
26 64 -13.47    -200 -605.1  606     imp:n=1 $ Top of Top Support Structure
27 64 -13.47    -200  305   -101 202 imp:n=1 $ Rest of Top Support Structure
28 64 -13.47    -309  201   -101 202 imp:n=1 $ Rest of Bottom Support Structure
c
c Fuel Pins
30 64 -13.47    -305  309          u=1 imp:n=1 $ Non-Fueled Portion of Core
31 64 -13.47     305 -200          u=1 imp:n=1 $ Top Support Structure NFP
32 64 -13.47    -309  201          u=1 imp:n=1 $ Bottom Support Structure NFP
33 11 -9.78192  -300 -306  307      u=2 imp:n=1 $ Fuel UO2
```

```
34 21 -2.95     -300  306 -305      u=2 imp:n=1 $ Top Axial Reflector
35 21 -2.95     -300 -307  308      u=2 imp:n=1 $ Bottom Axial Reflector
36 81 -0.000801 -300  304 -308  309 u=2 imp:n=1 $ Fission Gas Plenum
37 91 -19.43    -304 -308  309      u=2 imp:n=1 $ Fission Spring
38 64 -13.47    -302  305 -200      u=2 imp:n=1 $ Upper End Cap
39 64 -13.47    -302 -309  201      u=2 imp:n=1 $ Lower End Cap
40 81 -0.000801 -301 -305  309  300 u=2 imp:n=1 $ Gap
41 61 -13.459   -302 -305  309  301 u=2 imp:n=1 $ Cladding
42 71 -0.00668  -303  302 -200  201 u=2 imp:n=1 $ Channel
43 64 -13.47     303 -305  309      u=2 imp:n=1 $ Rest of Hex
44 64 -13.47     303  305 -200      u=2 imp:n=1 $ Top Support Structure
45 64 -13.47     303 -309  201      u=2 imp:n=1 $ Bottom Support Structure
c
c Core Block
50 0    -500 lat=2 u=9 imp:n=1
    fill=-12:12 -12:12 0:0
    1 1 1 1 1 1 1 1 1 1 1 1 1 1 1 1 1 1 1 1 1 1 1 1 1
     1 1 1 1 1 1 1 1 1 1 1 1 1 1 1 1 1 1 1 1 1 1 1 1
      1 1 1 1 1 1 1 1 1 1 1 1 2 2 2 2 2 2 2 2 2 1 1 1
       1 1 1 1 1 1 1 1 1 1 1 2 2 2 2 2 2 2 2 2 2 2 1 1
        1 1 1 1 1 1 1 1 1 1 2 2 2 2 2 2 2 2 2 2 2 2 1 1
         1 1 1 1 1 1 1 1 1 2 2 2 2 2 2 2 2 2 2 2 2 2 1 1
          1 1 1 1 1 1 1 1 2 2 2 2 2 2 2 2 2 2 2 2 2 2 1 1
           1 1 1 1 1 1 1 2 2 2 2 2 2 2 2 2 2 2 2 2 2 2 1 1
            1 1 1 1 1 1 2 2 2 2 2 2 2 2 2 2 2 2 2 2 2 2 1 1
             1 1 1 1 1 2 2 2 2 2 2 2 2 2 2 2 2 2 2 2 2 2 1 1
              1 1 1 1 2 2 2 2 2 2 1 1 1 1 2 2 2 2 2 2 2 1 1
               1 1 1 2 2 2 2 2 2 1 1 1 1 1 2 2 2 2 2 2 2 1 1
                1 1 2 2 2 2 2 2 1 1 1 1 1 1 2 2 2 2 2 2 1 1 1
                 1 1 2 2 2 2 2 2 1 1 1 1 1 2 2 2 2 2 2 2 1 1 1
                  1 1 2 2 2 2 2 2 1 1 1 1 1 2 2 2 2 2 2 2 1 1 1 1
                   1 1 2 2 2 2 2 2 1 1 1 1 2 2 2 2 2 2 2 1 1 1 1 1
                    1 1 2 2 2 2 2 2 2 2 2 2 2 2 2 2 2 2 2 1 1 1 1 1 1
                     1 1 2 2 2 2 2 2 2 2 2 2 2 2 2 2 2 2 1 1 1 1 1 1 1
                      1 1 2 2 2 2 2 2 2 2 2 2 2 2 2 2 2 2 1 1 1 1 1 1 1 1
                       1 1 2 2 2 2 2 2 2 2 2 2 2 2 2 2 2 1 1 1 1 1 1 1 1 1
                        1 1 2 2 2 2 2 2 2 2 2 2 2 2 2 2 2 1 1 1 1 1 1 1 1 1
                         1 1 1 2 2 2 2 2 2 2 2 2 2 2 2 2 1 1 1 1 1 1 1 1 1 1
                          1 1 1 1 1 1 1 1 1 1 1 1 1 1 1 1 1 1 1 1 1 1 1 1 1 1
                           1 1 1 1 1 1 1 1 1 1 1 1 1 1 1 1 1 1 1 1 1 1 1 1 1 1
c                                   S  C
c
51 0      -202  203 -200 201 fill=9 imp:n=1 $ Core Block
c
c Safety Pin
```

```
60 3  -2.2    -600 : -601           imp:n=1 $ Safety Pin
61 64 -13.47 -603    601 600.2      imp:n=1 $ Safety Pin Cladding Sph
62 64 -13.47  -602    600           imp:n=1 $ Safety Pin Cladding Cyl
63 0         -604   -606 602   603  imp:n=1 $ Safety Pin Clearance
64 64 -13.47  -605    604           imp:n=1 $ Safety Pin Thimble
c
c Reflectors
70 2 -3.01 -700 701          imp:n=1 $ Fixed Reflector
71 2 -3.01 -702 703  704  706 imp:n=1 $ Moving Reflector 1
72 2 -3.01 -702 703 -707  708 imp:n=1 $ Moving Reflector 2
73 2 -3.01 -702 703 -709  710 imp:n=1 $ Moving Reflector 3
74 2 -3.01 -702 703 -711  712 imp:n=1 $ Moving Reflector 4
75 2 -3.01 -702 703 -713  714 imp:n=1 $ Moving Reflector 5
76 2 -3.01 -702 703 -715  704 imp:n=1 $ Moving Reflector 6
77 2 -3.01 -702 703 -705 -707 imp:n=1 $ Moving Reflector 7
78 2 -3.01 -702 703  706 -709 imp:n=1 $ Moving Reflector 8
79 2 -3.01 -702 703  708 -711 imp:n=1 $ Moving Reflector 9
80 2 -3.01 -702 703  710 -713 imp:n=1 $ Moving Reflector 10
81 2 -3.01 -702 703  712 -715 imp:n=1 $ Moving Reflector 11
82 2 -3.01 -702 703  714 -705 imp:n=1 $ Moving Reflector 12
c
c Shield
90 4 -7.75 -900              imp:n=1 $ Shield
c ************************************

c ************************************
c
c Surfaces
c
c vessel Surfaces
100 cz  30.905          $ Vessel OR
101 cz  30.455          $ Vessel IR
102 pz  136.96          $ Top of Vessel Cylinder
103 pz  30.905          $ Bottom of Vessel Cylinder
104 sz  136.96 30.905     $ Top Dome OR
105 sz  136.96 30.455     $ Top Dome IR
106 sz  30.905 30.905     $ Bottom Dome OR
107 sz  30.905 30.455     $ Bottom Dome IR
108 rcc 0 0 136.96
       0 0 55.563
       30.905          $ Vessel Skirt IR
109 rcc 0 0 136.96
       0 0 55.563
       32.175          $ Vessel Skirt OR
110 sz  129.27 165       $ Space surrounding Craft
c
```

```
c Inner Core Structures Surfaces
200 pz 136.96           $ Top Support Structure
201 pz 30.905           $ Bottom Support Structure
202 cz 26.645           $ Block OR
203 cz 7.239           $ Block IR
204 sz 136.96 26.645      $ Inner Dome OR
205 sz 136.96 26.195      $ Inner Dome IR
c
c Fuel Pin Surfaces
300 cz 0.9247           $ Fuel Pellet OR
301 cz 0.9307           $ Gap OR
302 cz 0.9826           $ Clad OR
303 cz 1.1925           $ Channel OR
304 cz 0.7423           $ Fission Spring (Modeled as Cylinder)
305 pz 131.88           $ Top of Axial Reflector
306 pz 128.88           $ Top of Fuel
307 pz 68.080           $ Bottom of Fuel
308 pz 65.080           $ Bottom of Axial Reflector
309 pz 34.080           $ Bottom of Fission Gas Plenum
c
c Core Block Surfaces
500 rhp 0 0     30.905
       0 0     106.055
       0 1.307 0        $ Hexagonal Lattice Element
c
c Safety Pin Surfaces
600 rcc 0 0 0
       0 0 129.524
       6.36            $ Safety Pin Cylindrical Section
601 sz  129.524 6.36      $ Top Dome of Safety Pin
602 rcc 0 0 0
       0 0 129.524
       6.436           $ Safety Pin Cladding OR
603 sz  129.524 6.436     $ Safety Pin Cladding on Spherical portion
604 rcc 0 0 0
       0 0 135.96
       6.551           $ Safety Pin Clearance OR
605 rcc 0 0 0
       0 0 135.96
       6.932           $ Safety Pin Thimble OR
606 pz  135.96          $ Safety Pin Thimble Top
607 pz  0               $ Safety Pin Bottom
c
c Reflector Surfaces
700 rcc 0 0 118.544
       0 0 13.336
```

```
      42.55          $ Fixed Reflector OR
701 rcc 0 0 118.544
      0 0 13.336
      31.54          $ Fixed Reflector IR
702 rcc 0 0 65.080
      0 0 53.464
      42.55          $ Moving Reflector OR
703 rcc 0 0 65.080
      0 0 53.464
      31.54          $ Moving Reflector IR
704 px  0.3175          $ Plane Separating Moving Reflector 12&1/6$7
705 px -0.3175          $ Plane Separating Moving Reflector 12&1/6&7
706 p  -1.732 1 0  0.635  $ Plane Separating Moving Reflector 1&2/7&8
707 p  -1.732 1 0 -0.635  $ Plane Separating Moving Reflector 1&2/7&8
708 p  -0.577 1 0  0.3666 $ Plane Separating Moving Reflector 2&3/8&9
709 p  -0.577 1 0 -0.3666 $ Plane Separating Moving Reflector 2&3/8&9
710 py  0.3175          $ Plane Separating Moving Reflector 3&4/9&10
711 py -0.3175          $ Plane Separating Moving Reflector 3&4/9&10
712 p   0.577 1 0  0.3666 $ Plane Separating Moving Reflector 4&5/10&11
713 p   0.577 1 0 -0.3666 $ Plane Separating Moving Reflector 4&5/10&11
714 p   1.732 1 0  0.635  $ Plane Separating Moving Reflector 5&6/11&12
715 p   1.732 1 0 -0.635  $ Plane Separating Moving Reflector 5&6/11&12
c
c Shield Surfaces
c Shield is modeled as circular truncated cone, due to difficulty of modeling
c ellipses as faces of truncated cone
900 trc 0      0      258.553
      0      0     -66.03
      83.674 69.639     $ Shield truncated cone
c ************************************

c ************************************
c
c Materials
c
c UO2 93% enriched RT (10.111 g/cm3)
m1    92234       0.0071   92235       0.9300  92238       0.06289
      8016       2.0
c UO2 93% enriched 1389 (10.111 g/cm3)
m11   92234.94c 0.0071   92235.94c 0.9300  92238.94c 0.06289
      8016.94c 2.0
c UO2 93% enriched 1506 (10.111 g/cm3)
m12   92234.92c 0.0071   92235.92c 0.9300  92238.92c 0.06289
      8016.92c 2.0
c UO2 93% enriched 1628 (10.111 g/cm3)
m13   92234.90c 0.0071   92235.90c 0.9300   92238.90c 0.06289
```

```
      8016.90c 2.0
c BeO RT (3.01 g/cm3)
m2     4009       0.5       8016       0.5
mt2   beo.60t
c BeO 1150 (2.86 g/cm3)
m21    4009.90c 0.5       8016.90c 0.5
mt21  beo.60t
c B4C (95% enriched B10) (2.2 g/cm3)
m3     5010       0.76      5011       0.04      6000       0.20
c Be-B4C-W
m4     4009       0.333     5010       0.2533    5011       0.0133
       6000       0.0667    74182      0.0889    74183      0.0479
       74184      0.1022    74186      0.0943
c Alloy 617
m5    42000      -.09     28000      -.54     24000      -.22
      26000      -.01     22000      -.003    13027      -.012
      27059      -.125
c Mo-47.5Re Clad/Block RT
m6    42092      0.1037   42094      0.0644   42095      0.1114
      42096      0.1169   42097      0.0672   42098      0.1688
      42100      0.0672   75185      0.112    75187      0.1876
c Mo-47.5Re Clad 1389
m61   42092.95c 0.1037   42094.95c 0.0644   42095.95c 0.1114
      42096.95c 0.1169   42097.95c 0.0672   42098.95c 0.1688
      42100.95c 0.0672   75185.95c 0.112    75187.95c 0.1876
c Mo-47.5Re Clad 1506
m62   42092.93c 0.1037   42094.93c 0.0644   42095.93c 0.1114
      42096.93c 0.1169   42097.93c 0.0672   42098.93c 0.1688
      42100.93c 0.0672   75185.93c 0.112    75187.93c 0.1876
c Mo-47.5Re Clad 1628
m63   42092.91c 0.1037   42094.1231c 0.0644   42095.1231c 0.1114
      42096.91c 0.1169   42097.1231c 0.0672   42098.1231c 0.1688
      42100.91c 0.0672   75185.1231c 0.112    75187.1231c 0.1876
c Mo-47.5Re Block 1150
m64   42092.94c 0.1037   42094.94c 0.0644   42095.94c 0.1114
      42096.94c 0.1169   42097.94c 0.0672   42098.94c 0.1688
      42100.94c 0.0672   75185.94c 0.112    75187.94c 0.1876
c He/Xe RT 78/22 (0.0218 g/cm3)
m7     2004     0.78
      54129.94c 0.0619
      54131.94c 0.0498
      54132.94c 0.0631
      54134.94c 0.0245
      54136.94c 0.0207
c He/Xe 1150 78/22 (0.0218 g/cm3)
m71    2004.94c 0.78
```

```
     54129.94c 0.0619
     54131.94c 0.0498
     54132.94c 0.0631
     54134.94c 0.0245
     54136.94c 0.0207
c He RT
m8     2004       1.0
c He 1389
m81    2004.95c 1.0
c He 1506
m82    2004.93c 1.0
c He 1628
m83    2004.91c 1.0
c W-25Re RT
m9    74182      -.1845   74183      -.1073   74184      -.2303
     74186      -.2145   75185      -.0929   75187      -.1571
c W-25Re 1389
m91   74182.95c -.1845   74183.95c -.1073   74184.95c -.2303
     74186.95c -.2145   75185.95c -.0929   75187.95c -.1571
c W-25Re 1506
m92   74182.93c -.1845   74183.93c -.1073   74184.93c -.2303
     74186.93c -.2145   75185.93c -.0929   75187.93c -.1571
c W-25Re 1628
m93   74182.91c -.1845   74183.91c -.1073   74184.91c -.2303
     74186.91c -.2145   75185.91c -.0929   75187.91c -.1571
c
c Source Definition and Kcode
c
c sdef
kcode 1000 1.0 30 2030
ksrc -.02 .01 83.0
print
```

Appendix B: MATLAB Codes

Thermal Analysis: Calculating Heat Transfer Coefficients of Fluids (Produced by CDR Blair/edited by 1/C Allen)

```
clear
clc
close 'all'

%% Add current directory to the Python Path
EasyProp_path = ' '; %<- Path if EasyProp.py is in your current directory
if count(py.sys.path,EasyProp_path) == 0  % <-- see if desired directory is
on path
    insert(py.sys.path,int32(0),EasyProp_path); %<-- if not; add it.
end

%% Initialize Fluid Property object
fluid = 'He';
units = 'SI';
coolant = py.EasyProp.simpleFluid(fluid,units);

%% provide basic system parameters

T_in = 618; % C, from 891K given in Prometheus summary
T_out = 877; % C, from 1150K given in Prometheus summary and MIDN Allen work



% gas is actually He-0.784 / Xe-0.216 a/o

P_coolant = 2000; % kPa
% assume isobaric heat addition in Rx.
q_prime = 68.59*(1/1000)*(100); % W/cm -> kW/cm -> kW/m
L_channel = 0.608; % m, length of channel
Q_channel = q_prime*L_channel; % kW

r_fuel = 0.9095; % cm
t_gap = 0.022;% cm
t_clad = 0.051;% cm
t_coolant_channel = 0.216;% cm

Ro_channel = r_fuel+t_gap + t_clad+t_coolant_channel;% cm
Ri_channel = Ro_channel - t_coolant_channel;% cm

%% estimate coolant mass flow rate and velocity
h_cool_in = coolant.h_pT(P_coolant,T_in); % kJ/kg
h_cool_out = coolant.h_pT(P_coolant,T_out);
m_dot_coolant = Q_channel/(h_cool_out - h_cool_in); % kg/sec - estimated
coolant mass flow rate.
fprintf('Coolant mass flow rate = %g kg/sec \n',m_dot_coolant);

A_channel = pi*(Ro_channel^2 - Ri_channel^2)*((1/100)^2);% cm^2 --> m^2
```

```
T_ave = (T_in + T_out)/2;

v_coolant = coolant.v_pT(P_coolant,T_ave); % m^3/kg - coolant specific volume
rho_coolant = 1/v_coolant; % kg/m^3 - coolant density
rho_coolant_mcnp=(rho_coolant)/((100^3)/1000); %coolant density in g/cc
fprintf('The density of coolant is %g g/cc\n',rho_coolant_mcnp)

v_coolant_avg = m_dot_coolant/(A_channel*rho_coolant); % m/sec

fprintf('Average coolant velocity = %g m/sec \n',v_coolant_avg);

%% Estimate coolant Reynolds number and Prandtl number
Pr_coolant = coolant.Prandtl_pT(P_coolant,T_ave); %Prandtl number

P_w = 2*pi*(Ro_channel + Ri_channel)*((1/100)); % cm^2 -> m^2, wetted
perimeter

D_hyd = (4*A_channel/P_w); % m -> cm, hydraulic diameter (took out *100)
keeps it m

mu_coolant = coolant.mu_pT(P_coolant,T_ave); % kg/m-s (Pa-s) dynamic
viscosity of the coolant

Re_coolant = rho_coolant*v_coolant_avg*D_hyd/mu_coolant; % Reynolds number of
the coolant
fprintf('The Reynolds number is %5.4e\n', Re_coolant)

%% estimate convective heat transfer coefficient using Dittus-Boelter

Nu_DB = @(Re,Pr) 0.023*(Re^(0.8))*(Pr^(0.4)); % see Eqn 10.91 of Todreas

Nu_coolant_DB = Nu_DB(Re_coolant,Pr_coolant);

k_coolant = coolant.k_pT(P_coolant,T_ave)*(1000/100); % kW/m-K -> W/cm-K

h_coolant_DB = Nu_coolant_DB*k_coolant/(D_hyd*100); % W/cm^2-k
fprintf('h_coolant using Dittus-Boelter (Eq 10.91) = %g W/cm^2-K \n',...
    h_coolant_DB);

Nu_Gn = @(Re,Pr) 0.0214*((Re^0.8) - 100)*(Pr^0.4);

Nu_coolant_Gn = Nu_Gn(Re_coolant,Pr_coolant);
h_coolant_Gn = Nu_coolant_Gn*k_coolant/(D_hyd*100); % W/cm^2-k
fprintf('h_coolant using Gnielinski (Eq 10.97a) = %g W/cm^2-K \n',...
    h_coolant_Gn);
```

Thermal Expansion: Solid Density and Volume Change Calculations (UO_2)

```
%% Establish Variables
% Guide to Vectors
% (Vessel Block Clad Radial_Ref Axial_Ref Safety_Pin Fission_Spring)
% Temeperature Needed in Calculation
% (K C C C C C C)
```

```
CTE_UO2=[12.01e-6 12.56e-6 13.18e-6]; %(um/mK) Coefficient of Thermal
Expansion for UO2
PCT_UO2=[1389 1506 1628]; %(K) Peak Core Temperatures measured
CTE=[11.6e-6 6.45e-6 6.45e-6 6.4e-6 7.2e-6 5.0e-6 5.04e-6]; %(um/mC)
Coeffeicient of Thermal Expansion for other materials
T_1389=[20 877 918 20 877 20 918]; %(C) Temperature of Materials for 1389 PCT
T_1506=[20 877 938 20 877 20 938]; %(C) Temperature of Materials for 1506 PCT
T_1628=[20 877 958 20 877 20 958]; %(C) Temperature of Materials for 1628 PCT
rho_UO2=10.111; %(g/cc) room temperature density of UO2
rho=[8.498 13.7 13.7 3.01 3.01 2.2 19.7]; %(g/cc) room temperature density of
other materials
n_fp=288; %Number of Fuel Pins
r_ov=30.905; %(cm) Outer Vessel Radius
t_v=0.45; %(cm) Outer Vessel Thickness
r_ob=26.645; %(cm) Block Outer Radius
r_ib=7.239; %(cm) Block Inner Radius
r_f=0.9095; %(cm) Fuel Pellet Outer Radius
t_g=0.022; %(cm) Gap Thickness
t_cl=0.051; %(cm) Clad Thickness
t_ch=0.216; %(cm) Channel (Coolant) Thickness
r_sp=6.36; %(cm) Safety Pin Outer Radius
t_spcl=0.076; %(cm) Safety Pin Cladding Thickness
r_spth=6.932; %(cm) Safety Pin Thimble Outer Radius
r_fs=0.7372; %(cm) Fuel Spring Outer Radius
r_uc=1.509; %(cm) Side Length of Hexagonal Unit Cell
h_f=60.8; %(cm) Fuel Height
h_gp=31; %(cm) Fission Gas Plenum Height
h_ar=3; %(cm) Axial Reflector Height
h_fp=h_f+h_gp+(2*h_ar); %(cm) Total Height of the Fuel Pin

%Establishing Radii
r_g=r_f+t_g; %(cm) Outer Radius of Gap
r_cl=r_g+t_cl; %(cm) Outer Radius of Clad
r_ch=r_cl+t_ch; %(cm) Outer Radius of Channel

%% Density Calculations for 1389K PCT
fprintf('(Vessel Block Clad Radial_Ref Axial_Ref Safety_Pin Fission_Spring)')
rho_1389_UO2=rho_UO2./((1+(CTE_UO2(1)*PCT_UO2(1))).^2) %(g/cc) new density
for UO2
rho_1389=rho./((1+(CTE.*T_1389)).^3) % (g/cc) new densities for 1389 PCT

%Calculating Volume Change of Fuel for 1389K PCT
vol_UO2=pi*(r_f^2)*h_f; %(cc) Volume of fuel
m_UO2=rho_UO2*vol_UO2; %(g) mass of fuel
vol_1389_UO2=m_UO2/rho_1389_UO2 %(cc) Expanded Volume of Fuel
r_1389_f=sqrt(vol_1389_UO2/(pi*h_f)) %(cm) Expanded Radius of Fuel
%Check, if value is close to 1, radius and density are correct
fcheck_1389=((r_1389_f^2)*rho_1389_UO2)/((r_f^2)*rho_UO2);
fprintf('The Check is %5.5f\n', fcheck_1389)

%Calculating Volume Change of Fission Spring
vol_fs=pi*(r_fs^2)*h_gp; %(cc) Volume of Fission Spring
m_fs=rho(7)*vol_fs; %(g) mass of fission spring
vol_1389_fs=m_fs/rho_1389(7) %(cc) Expanded Volume of Fission Spring
r_1389_fs=sqrt(vol_1389_fs/(pi*h_gp)) %(cm) Expanded Radius of Fission Spring
```

```
%Calculating Volume Change of Clad for 1389K PCT
vol_cl=pi*(r_cl^2-r_g^2)*(h_fp); %(cc) Volume of clad
m_cl=rho(3).*vol_cl; %(g) mass of clad
vol_1389_cl=m_cl./rho_1389(3) %(cc) Expanded Volume of Clad
r_cl_cent=(r_cl+r_g)/2; %(cm)center radius of clad
r_1389_g=sqrt(r_cl_cent^2-((vol_1389_cl/2)/(pi*(h_fp)))) %(cm) Expanded Outer
Radius of Gap
r_1389_cl=sqrt(((vol_1389_cl/2)/(pi*(h_fp)))+r_cl_cent^2) %(cm) Expanded
Outer Radius of Clad
t_1389_cl=r_1389_cl-r_1389_g %(cm) Expanded thickness of clad
t_1389_g=r_1389_g-r_1389_f %(cm) Expanded thicknss of gap

%Calculating Volume Change of Block for 1389K PCT
vol_ch=pi*(r_ch^2)*(h_fp); %(cc) Volume of channel
tot_vol_ch=(n_fp*vol_ch); %(cc) Total Volume of all Channels
vol_b=(pi*(r_ob^2-r_ib^2)*h_fp)-(tot_vol_ch); %Volume of Block
vol_uc=vol_b/n_fp; %(cc) Volume of Unit Cell
m_b=rho(2).*vol_b; %(g) mass of block
vol_1389_b=m_b./rho_1389(2) %(cc) Expanded Volume of block
vol_1389_ch=(vol_1389_b/(n_fp)) %(cc) Expanded Volume for each Channel
diff_1389_vol=vol_1389_ch-vol_uc %(cc) Difference in Volume
r_1389_ch=sqrt((r_ch^2)-(diff_1389_vol/(pi*h_fp))) %(cm)Expanded Outer Radius
of Channel
t_1389_ch=r_1389_ch-r_1389_cl %(cm) Expanded thickness of Channel

%Ensuring Mass Conservation of Gap
vol_g=pi*h_fp*((r_g^2)-(r_f^2)); %(cc) Volume of Gap surrounding fuel
vol_1389_g=pi*h_fp*((r_1389_g^2)-(r_1389_f^2));%(cc) Volume of Gap
surrounding fuel
rho_g=0.033; %(g/cc) Density of Unheated Gas
rho_1389_g=0.000801; %(g/cc) Density of Heated Gas
m_g=vol_g*rho_g
m_1389_g=vol_1389_g*rho_1389_g

%% Density and Volume Change Calc for 1506 PCT
fprintf('(Vessel Block Clad Radial_Ref Axial_Ref Safety_Pin Fission_Spring)')
rho_1506_UO2=rho_UO2./((1+(CTE_UO2(2)*PCT_UO2(2))).^2) %(g/cc) new density
for UO2
rho_1506=rho./((1+(CTE.*T_1506)).^3) %(g/cc) new densities for 1604 PCT

%Calculating Volume Change of Fuel for 1506K PCT
vol_UO2=pi*(r_f^2)*h_f; %(cc) Volume of fuel
m_UO2=rho_UO2*vol_UO2; %(g) mass of fuel
vol_1506_UO2=m_UO2/rho_1506_UO2 %(cc) Expanded Volume of Fuel
r_1506_f=sqrt(vol_1506_UO2/(pi*h_f)) %(cm) Expanded Radius of Fuel
%Check, if value is close to 1, radius and density are correct
fcheck_1506=((r_1506_f^2)*rho_1506_UO2)/((r_f^2)*rho_UO2);
fprintf('The Check is %5.5f\n', fcheck_1506)

%Calculating Volume Change of Fission Spring
vol_fs=pi*(r_fs^2)*h_gp; %(cc) Volume of Fission Spring
m_fs=rho(7)*vol_fs; %(g) mass of fission spring
vol_1506_fs=m_fs/rho_1506(7) %(cc) Expanded Volume of Fission Spring
r_1506_fs=sqrt(vol_1506_fs/(pi*h_gp)) %(cm) Expanded Radius of Fission Spring

%Calculating Volume Change of Clad for 1506K PCT
```

```
vol_cl=pi*(r_cl^2-r_g^2)*(h_fp); %(cc) Volume of clad
m_cl=rho(3).*vol_cl; %(g) mass of clad
vol_1506_cl=m_cl./rho_1506(3) %(cc) Expanded Volume of Clad
r_cl_cent=(r_cl+r_g)/2; %(cm)center radius of clad
r_1506_g=sqrt(r_cl_cent^2-((vol_1506_cl/2)/(pi*(h_fp)))) %(cm) Expanded Outer
Radius of Gap
r_1506_cl=sqrt(((vol_1506_cl/2)/(pi*(h_fp)))+r_cl_cent^2) %(cm) Expanded
Outer Radius of Clad
t_1506_cl=r_1506_cl-r_1506_g %(cm) Expanded thickness of clad
t_1506_g=r_1506_g-r_1506_f %(cm) Expanded thicknss of gap

%Calculating Volume Change of Block for 1506K PCT
vol_ch=pi*(r_ch^2)*(h_fp); %(cc) Volume of channel
tot_vol_ch=(n_fp*vol_ch); %(cc) Total Volume of all Channels
vol_b=(pi*(r_ob^2-r_ib^2)*h_fp)-(tot_vol_ch); %Volume of Block
vol_uc=vol_b/n_fp %(cc) Volume of Unit Cell
m_b=rho(2).*vol_b; %(g) mass of block
vol_1506_b=m_b./rho_1506(2) %(cc) Expanded Volume of block
vol_1506_ch=(vol_1506_b/(n_fp)) %(cc) Expanded Volume for each Channel
diff_1506_vol=vol_1506_ch-vol_uc %(cc) Difference in Volume
r_1506_ch=sqrt((r_ch^2)-(diff_1506_vol/(pi*h_fp))) %(cm)Expanded Outer Radius
of Channel
t_1506_ch=r_1506_ch-r_1506_cl %(cm) Expanded thickness of Channel

%% Density and Volume Change Calc for 1628 PCT
fprintf('(Vessel Block Clad Radial_Ref Axial_Ref Safety_Pin Fission_Spring)')
rho_1628_UO2=rho_UO2./((1+(CTE_UO2(3)*PCT_UO2(3))).^2) %(g/cc) new density
for UO2
rho_1628=rho./((1+(CTE.*T_1628)).^3) %(g/cc) new densities for 1628 PCT

%Calculating Volume Change of Fuel for 1628K PCT
vol_UO2=pi*(r_f^2)*h_f; %(cc) Volume of fuel
m_UO2=rho_UO2*vol_UO2; %(g) mass of fuel
vol_1628_UO2=m_UO2/rho_1628_UO2 %(cc) Expanded Volume of Fuel
r_1628_f=sqrt(vol_1628_UO2/(pi*h_f)) %(cm) Expanded Radius of Fuel
%Check, if value is close to 1, radius and density are correct
fcheck_1628=((r_1628_f^2)*rho_1628_UO2)/((r_f^2)*rho_UO2);
fprintf('The Check is %5.5f\n', fcheck_1628)

%Calculating Volume Change of Fission Spring
vol_fs=pi*(r_fs^2)*h_gp; %(cc) Volume of Fission Spring
m_fs=rho(7)*vol_fs; %(g) mass of fission spring
vol_1628_fs=m_fs/rho_1628(7) %(cc) Expanded Volume of Fission Spring
r_1628_fs=sqrt(vol_1628_fs/(pi*h_gp)) %(cm) Expanded Radius of Fission Spring

%Calculating Volume Change of Clad for 1628K PCT
vol_cl=pi*(r_cl^2-r_g^2)*(h_fp); %(cc) Volume of clad
m_cl=rho(3).*vol_cl; %(g) mass of clad
vol_1628_cl=m_cl./rho_1628(3) %(cc) Expanded Volume of Clad
r_cl_cent=(r_cl+r_g)/2; %(cm)center radius of clad
r_1628_g=sqrt(r_cl_cent^2-((vol_1628_cl/2)/(pi*(h_fp)))) %(cm) Expanded Outer
Radius of Gap
r_1628_cl=sqrt(((vol_1628_cl/2)/(pi*(h_fp)))+r_cl_cent^2) %(cm) Expanded
Outer Radius of Clad
t_1628_cl=r_1628_cl-r_1628_g %(cm) Expanded thickness of clad
t_1628_g=r_1628_g-r_1628_f %(cm) Expanded thicknss of gap
```

```
%Calculating Volume Change of Block for 1628K PCT
vol_ch=pi*(r_ch^2)*(h_fp); %(cc) Volume of channel
tot_vol_ch=(n_fp*vol_ch); %(cc) Total Volume of all Channels
vol_b=(pi*(r_ob^2-r_ib^2)*h_fp)-(tot_vol_ch); %Volume of Block
vol_uc=vol_b/n_fp %(cc) Volume of Unit Cell
m_b=rho(2).*vol_b; %(g) mass of block
vol_1628_b=m_b./rho_1628(2) %(cc) Expanded Volume of block
vol_1628_ch=(vol_1628_b/(n_fp)) %(cc) Expanded Volume for each Channel
diff_1628_vol=vol_1628_ch-vol_uc %(cc) Difference in Volume
r_1628_ch=sqrt((r_ch^2)-(diff_1628_vol/(pi*h_fp))) %(cm)Expanded Outer Radius
of Channel
t_1628_ch=r_1628_ch-r_1628_cl %(cm) Expanded thickness of Channel
```

Thermal Expansion: Calculating Density of Fluid Materials (Produced by CDR Blair)

```
%% Add current directory to the Python Path
EasyProp_path = ' '; %<- Path if EasyProp.py is in your current directory
if count(py.sys.path,EasyProp_path) == 0  % <-- see if desired directory is
on path
    insert(py.sys.path,int32(0),EasyProp_path); %<-- if not; add it.
end

%%
He_gap=1.0;
Xe_gap=0.0;
HeXe_mixture = py.dict(pyargs('He',He_gap,'Xenon',Xe_gap));
units = 'SI';% alternatively use 'USCS'
weight = 'a/o'; % alternatively use 'w/o' for weight percent

HeXe = py.EasyProp.simpleMixture(HeXe_mixture,weight,units);

T = (1248-273); % C
P = 2000; % kPa

specVol = HeXe.v_pT(P,T);

rho = (1/specVol)/((100^3)/1000);
fprintf('Density at %g C, %g kPa is: %g g/{cm^3} \n',T,P,rho);
```

Results: Producing Plots for BOL Base Case k_{eff} Analysis

```
%% Establish Variables
T=[293 1389 1506 1628]; %(K) Peak Core Temperature
keff=[0.98987 0.98089 0.98024 0.97984];%Effective Multplication Factor
alpha_T=NaN(4,1);
for i=2:4
    alpha_T(i)=(keff(i)-keff(i-1))/(T(i)-T(i-1)); %Temperature Coeffcient of
Rx
end
data=table(T',keff',alpha_T,'VariableNames',{'Temperature','keff',...
    'alpha_T'})
tbl2=table(T',alpha_T,'VariableNames',{'Temperature','Alpha_T'});
```

```
err=[0.00042 0.00041 0.00042 0.00041];
errorbar(T,keff,err,'-o','LineWidth',2)
title('Base Case BOL Keff')
xlabel('Peak Core Temperature (K)')
ylabel('Effective Multiplication Factor')
grid on
axis([250 1650 0.979 0.991])
tbl=table(T',keff','VariableNames',{'Temperature','keff'});
lm=fitlm(tbl,'linear')
alpha_T_eqn=fitlm(tbl2,'linear')
```

Mass Comparison:

```
clear
close all
clc

%% Establishing UO2/UN/UC Parameters
n=288;
rho_un=14.32; %(g/cc) UN Density
rho_uo2=10.111; %(g/cc) UO2 Density
rho_uc=13.63; %(g/cc) UC Density
rho_more=13.7; %(g/cc) Mo-47.5Re Density
rho_fs85=10.6; %(g/cc) FS-85 Density
rho_re=21.07; %(g/cc) Re Density
rho_beo=3.01; %(g/cc) BeO Density
rho_a617=8.498; %(g/cc) Alloy 617 Density
rho_b4c=2.2; %(g/cc) B4C Density
rho_WRe=19.73; %(g/cc) W-25Re Density
h_f=60.8; %(cm) Height of Fuel
h_uc=97.8; %(cm) Height of Unit Cell
h_ss=8.255; %(cm) Height of Support Structure
h_ar=6; %(cm) Height of Axial Reflectors
h_rr=66.8; %(cm) Height of Radial Reflectors
h_sp_un=130.331; %(cm) Height of Safety Pin
h_sp_bc=129.524; %(cm) Height of Safety Pin
h_sp_uc=130.264; %(cm) Height of Safety Pin
h_spt=135.96; %(cm) Height of Safety Pin Thimble
h_ves=106.055; %(cm) Height of Vessel
r_f_un=0.7109; %(cm) Radius of UN Fuel
r_l_un=0.7309; %(cm) Liner OR
r_g_un=0.7529; %(cm) Gap OR
r_cl_un=0.8039; %(cm) Clad OR
r_ch_un=1.0565; %(cm) Channel OR
r_block_un=(2/sqrt(3))*1.141; %(cm) Block Side Length
r_fs_un=0.5755; %(cm) Fission Spring OR
ir_rr_un=28.63; %(cm) Radial Reflector IR
or_rr_un=39.64; %(cm) Radial Reflector OR
r_sp_un=5.553; %(cm) Safety Pin OR
r_spc_un=5.629; %(cm) Safety Pin Clad OR
r_spt_un=5.966; %(cm) Safety Pin Thimble OR
ir_b_un=6.32; %(cm) Block IR
or_ves_un=27.993; %(cm) Vessel OR
ir_ves_un=27.543; %(cm) Vessel IR
or_idome_un=23.261; %(cm) Inner Dome OR
ir_idome_un=22.811; %(cm) Inner Dome IR
v_f_un=pi*(r_f_un^2)*h_f; %(cm3) Vol of Fuel
```

```
v_l_un=pi*((r_l_un^2)-(r_f_un^2))*h_f; %(cm3) Volume of Liner
v_cl_un=pi*((r_cl_un^2)-(r_g_un^2))*h_uc; %(cm3) Volume of Clad
v_ch_un=pi*(r_ch_un^2)*h_uc; %(cm3) Vol of Fuel
v_b_un=(pi*((or_idome_un^2)-(ir_b_un^2))*h_uc)-(n*v_ch_un); %(cm3)
v_r_un=pi*(r_f_un^2)*h_ar; %(cm3) Vol of Axial Reflectors
v_fs_un=pi*(r_fs_un^2)*(h_uc-h_f-h_ar); %(cm3) Vol of Fission Spring
v_rr_un=pi*((or_rr_un^2)-(ir_rr_un^2))*h_rr; %(cm3) Volume of Radial Ref
v_ves_un=(pi*((or_ves_un^2)-(ir_ves_un^2))*h_ves)+...
    (pi*(4/3)*((or_ves_un^2)-(ir_ves_un^2)))+...
    (0.5*pi*(4/3)*((or_idome_un^2)-(ir_idome_un^2))); %(cm3) Vol of Vessel
v_sp_un=(pi*(r_sp_un^2)*h_sp_un)+((4/3)*pi*(r_sp_un^3)); %(cm3) Vol of SP
v_spc_un=(pi*((r_spc_un^2)-(r_sp_un^2))*h_sp_un)+...
    ((4/3)*pi*((r_spc_un^3)-(r_sp_un^3))); %(cm3) Vol of SP
v_spt_un=(pi*((r_spt_un^2)-(r_spc_un^2))*h_sp_un); %(cm3) Vol of SP Thimble
v_ss_un=pi*(or_idome_un^2)*h_ss; %(cm3) Volume of Support Structures
m_f_un=v_f_un*n*rho_un/1000;
fprintf('The mass of UN fuel is %5.2f kg\n',m_f_un)
m_l_un=v_l_un*n*rho_re/1000;
fprintf('The mass of UN liner is %5.2f kg\n',m_l_un)
m_cl_un=v_cl_un*n*rho_fs85/1000;
fprintf('The mass of UN clad is %5.2f kg\n',m_cl_un)
m_b_un=v_b_un*rho_fs85/1000;
fprintf('The mass of UN block is %5.2f kg\n',m_b_un)
m_r_un=((v_r_un*n)+v_rr_un)*rho_beo/1000;
fprintf('The mass of UN Reflectors is %5.2f kg\n',m_r_un)
m_fs_un=v_fs_un*n*rho_WRe/1000;
fprintf('The mass of UN fission spring is %5.2f kg\n',m_fs_un)
m_ves_un=v_ves_un*rho_a617/1000;
fprintf('The mass of UN vessel is %5.2f kg\n',m_ves_un)
m_sp_un=(v_sp_un*rho_b4c)/1000;
m_spc_un=(v_spc_un*rho_fs85)/1000;
m_spt_un=(v_spt_un*rho_fs85)/1000;
m_sp_all_un=((v_sp_un*rho_b4c)+(v_spc_un*rho_fs85)+...
    (v_spt_un*rho_fs85))/1000;
fprintf('The mass of all UN Safety Pin pieces is %5.2f kg\n',m_sp_all_un)
m_ss_un=(v_ss_un*rho_fs85)/1000;
fprintf('The mass of UN Support Structures is %5.2f kg\n',m_ss_un)
m_tot_un=m_f_un+m_l_un+m_cl_un+m_b_un+m_r_un+m_fs_un+m_ves_un+...
    m_sp_all_un+m_ss_un;
fprintf('The total mass of UN is %5.2f kg\n',m_tot_un)
%UO2
r_f_bc=0.9095; %(cm) Radius of Base Case Fuel
r_g_bc=0.932; %(cm) Gap OR
r_cl_bc=0.983; %(cm) Clad OR
r_ch_bc=1.199; %(cm) Channel OR
r_block_bc=(2/sqrt(3))*1.307; %(cm) Block Side Length
r_fs_bc=0.7372; %(cm) Fission Spring OR
ir_rr_bc=31.54; %(cm) Radial Reflector IR
or_rr_bc=42.55; %(cm) Radial Reflector OR
r_sp_bc=6.36; %(cm) Safety Pin OR
r_spc_bc=6.436; %(cm) Safety Pin Clad OR
r_spt_bc=6.932; %(cm) Safety Pin Thimble OR
ir_b_bc=7.239; %(cm) Block IR
or_ves_bc=30.905; %(cm) Vessel OR
ir_ves_bc=30.455; %(cm) Vessel IR
or_idome_bc=26.645; %(cm) Inner Dome OR
ir_idome_bc=26.195; %(cm) Inner Dome IR
```

```
v_f_bc=pi*(r_f_bc^2)*h_f; %(cm3) Vol of Fuel
v_cl_bc=pi*((r_cl_bc^2)-(r_g_bc^2))*h_uc; %(cm3) Volume of Clad
v_ch_bc=pi*(r_ch_bc^2)*h_uc; %(cm3) Vol of Fuel
v_b_bc=(pi*((or_idome_bc^2)-(ir_b_bc^2))*h_uc)-(n*v_ch_bc); %(cm3)
v_r_bc=pi*(r_f_bc^2)*h_ar; %(cm3) Vol of Axial Reflectors
v_fs_bc=pi*(r_fs_bc^2)*(h_uc-h_f-h_ar); %(cm3) Vol of Fission Spring
v_rr_bc=pi*((or_rr_bc^2)-(ir_rr_bc^2))*h_rr; %(cm3) Volume of Radial Ref
v_ves_bc=(pi*((or_ves_bc^2)-(ir_ves_bc^2))*h_ves)+...
    (pi*(4/3)*((or_ves_bc^2)-(ir_ves_bc^2)))+...
    (0.5*pi*(4/3)*((or_idome_bc^2)-(ir_idome_bc^2))); %(cm3) Vol of Vessel
v_sp_bc=(pi*(r_sp_bc^2)*h_sp_bc)+((4/3)*pi*(r_sp_bc^3)); %(cm3) Vol of SP
v_spc_bc=(pi*((r_spc_bc^2)-(r_sp_bc^2))*h_sp_bc)+...
    ((4/3)*pi*((r_spc_bc^3)-(r_sp_bc^3))); %(cm3) Vol of SP
v_spt_bc=(pi*((r_spt_bc^2)-(r_spc_bc^2))*h_sp_un); %(cm3) Vol of SP Thimble
v_ss_bc=pi*(or_idome_bc^2)*h_ss; %(cm3) Volume of Support Structures
m_f_bc=v_f_bc*n*rho_un/1000;
fprintf('\nThe mass of Base Case fuel is %5.2f kg\n',m_f_bc)
m_cl_bc=v_cl_bc*n*rho_more/1000;
fprintf('The mass of Base Case clad is %5.2f kg\n',m_cl_bc)
m_b_bc=v_b_bc*rho_more/1000;
fprintf('The mass of Base Case block is %5.2f kg\n',m_b_bc)
m_r_bc=((v_r_bc*n)+v_rr_bc)*rho_beo/1000;
fprintf('The mass of Base Case Reflectors is %5.2f kg\n',m_r_bc)
m_fs_bc=v_fs_bc*n*rho_WRe/1000;
fprintf('The mass of Base Case fission spring is %5.2f kg\n',m_fs_bc)
m_ves_bc=v_ves_bc*rho_a617/1000;
fprintf('The mass of UN vessel is %5.2f kg\n',m_ves_bc)
m_sp_bc=(v_sp_bc*rho_b4c)/1000;
m_spc_bc=(v_spc_bc*rho_more)/1000;
m_spt_bc=(v_spt_bc*rho_more)/1000;
m_sp_all_bc=((v_sp_bc*rho_b4c)+(v_spc_bc*rho_more)+...
    (v_spt_bc*rho_more))/1000;
fprintf('The mass of all UN Safety Pin pieces is %5.2f kg\n',m_sp_all_bc)
m_ss_bc=(v_ss_bc*rho_more)/1000;
fprintf('The mass of UN Support Structures is %5.2f kg\n',m_ss_bc)
m_tot_bc=m_f_bc+m_cl_bc+m_b_bc+m_r_bc+m_fs_bc+m_ves_bc+m_sp_all_bc+m_ss_bc;
fprintf('The total mass of Base Case is %5.2f kg\n',m_tot_bc)
%UC
r_f_uc=0.7258; %(cm) Radius of UC Fuel
r_l_uc=0.7458; %(cm) Liner OR
r_g_uc=0.7678; %(cm) Gap OR
r_cl_uc=0.8188; %(cm) Clad OR
r_ch_uc=1.0687; %(cm) Channel OR
r_block_uc=(2/sqrt(3))*1.155; %(cm) Block Side Length
r_fs_uc=0.5883; %(cm) Fission Spring OR
ir_rr_uc=28.87; %(cm) Radial Reflector IR
or_rr_uc=39.88; %(cm) Radial Reflector OR
r_sp_uc=5.6202; %(cm) Safety Pin OR
r_spc_uc=5.696; %(cm) Safety Pin Clad OR
r_spt_uc=6.047; %(cm) Safety Pin Thimble OR
ir_b_uc=6.397; %(cm) Block IR
or_ves_uc=28.868; %(cm) Vessel OR
ir_ves_uc=27.783; %(cm) Vessel IR
or_idome_uc=23.544; %(cm) Inner Dome OR
ir_idome_uc=23.094; %(cm) Inner Dome IR
v_f_uc=pi*(r_f_uc^2)*h_f; %(cm3) Vol of Fuel
v_l_uc=pi*((r_l_uc^2)-(r_f_uc^2))*h_f; %(cm3) Volume of Liner
```

```
v_cl_uc=pi*((r_cl_uc^2)-(r_g_uc^2))*h_uc; %(cm3) Volume of Clad
v_ch_uc=pi*(r_ch_uc^2)*h_uc; %(cm3) Vol of Fuel
v_b_uc=(pi*((or_idome_uc^2)-(ir_b_uc^2))*h_uc)-(n*v_ch_uc); %(cm3)
v_r_uc=pi*(r_f_uc^2)*h_ar; %(cm3) Vol of Axial Reflectors
v_fs_uc=pi*(r_fs_uc^2)*(h_uc-h_f-h_ar); %(cm3) Vol of Fission Spring
v_rr_uc=pi*((or_rr_uc^2)-(ir_rr_uc^2))*h_rr; %(cm3) Volume of Radial Ref
v_ves_uc=(pi*((or_ves_uc^2)-(ir_ves_uc^2))*h_ves)+...
    (pi*(4/3)*((or_ves_uc^2)-(ir_ves_uc^2)))+...
    (0.5*pi*(4/3)*((or_idome_uc^2)-(ir_idome_uc^2))); %(cm3) Vol of Vessel
v_sp_uc=(pi*(r_sp_uc^2)*h_sp_uc)+((4/3)*pi*(r_sp_uc^3)); %(cm3) Vol of SP
v_spc_uc=(pi*((r_spc_uc^2)-(r_sp_uc^2))*h_sp_uc)+...
    ((4/3)*pi*((r_spc_uc^3)-(r_sp_uc^3))); %(cm3) Vol of SP
v_spt_uc=(pi*((r_spt_uc^2)-(r_spc_uc^2))*h_sp_uc); %(cm3) Vol of SP Thimble
v_ss_uc=pi*(or_idome_uc^2)*h_ss; %(cm3) Volume of Support Structures
m_f_uc=v_f_uc*n*rho_uc/1000;
fprintf('\nThe mass of UC fuel is %5.2f kg\n',m_f_uc)
m_l_uc=v_l_uc*n*rho_re/1000;
fprintf('The mass of UC liner is %5.2f kg\n',m_l_uc)
m_cl_uc=v_cl_uc*n*rho_fs85/1000;
fprintf('The mass of UC clad is %5.2f kg\n',m_cl_uc)
m_b_uc=v_b_uc*rho_fs85/1000;
fprintf('The mass of UC block is %5.2f kg\n',m_b_uc)
m_r_uc=((v_r_uc*n)+v_rr_uc)*rho_beo/1000;
fprintf('The mass of UC Reflectors is %5.2f kg\n',m_r_uc)
m_fs_uc=v_fs_uc*n*rho_WRe/1000;
fprintf('The mass of UC fission spring is %5.2f kg\n',m_fs_uc)
m_ves_uc=v_ves_uc*rho_a617/1000;
fprintf('The mass of UC vessel is %5.2f kg\n',m_ves_uc)
m_sp_uc=(v_sp_uc*rho_b4c)/1000;
m_spc_uc=(v_spc_uc*rho_fs85)/1000;
m_spt_uc=(v_spt_uc*rho_fs85)/1000;
m_sp_all_uc=((v_sp_uc*rho_b4c)+(v_spc_uc*rho_fs85)+...
    (v_spt_uc*rho_fs85))/1000;
fprintf('The mass of all UC Safety Pin pieces is %5.2f kg\n',m_sp_all_uc)
m_ss_uc=(v_ss_uc*rho_fs85)/1000;
fprintf('The mass of UC Support Structures is %5.2f kg\n',m_ss_uc)
m_tot_uc=m_f_uc+m_l_uc+m_cl_uc+m_b_uc+m_r_uc+m_fs_uc+m_ves_uc+...
    m_sp_all_uc+m_ss_uc;
fprintf('The total mass of UC is %5.2f kg\n',m_tot_uc)
```

Appendix C: ZAID and MAKXSF Description

In order to define materials within MCNP, a number called a ZAID number is used in the materials section of this code. The ZAID number is described below in Table C.1.

Table C.1: Description of ZAID Numbers

Sections of ZAID Number	Description of Sections
ZZAAA.##c	This is the element's Atomic Number, or how many protons the element has
ZZAAA.##c	This is the element's Atomic Mass, the combined number of protons and neutrons, important step in classifying which isotope of the element is being used
ZZAAA.##c	This is an identifier as there are typically many versions of any isotope. Example of how this is used is to distinguish between different temperatures
ZZAAA.##c	Having a "c" indicates that this cross section relies on continuous cross section neutrons

An example of one such ZAID number used in this application is 8016.80c. This applies to Oxygen which has 8 protons and 8 neutrons, leading to an atomic number of 8 and atomic mass of 16. The .80c signifies that the cross section is for 300K and is in the continuous spectrum of neutrons.

While this variety of ZAID numbers are helpful, these values only come in set temperatures (e.g., 300, 600, 900, 1600, and 2500K). These values are close to many of the temperatures necessary to the project, but in order to get more exact values, a methodology was developed to create cross sections for desired temperatures.

This process was accomplished through the use of MAKXSF. MAKXSF is a program that creates separate cross section directories for use within an MCNP run [19]. In addition, this program can be used to implement the Doppler broadening and make new cross sections.

MAKXSF is built into MCNP and uses existing cross sections to make cross sections at the desired temperatures for each study. These new cross sections are created by making a specs file. An example specs file is included below in Figure C.1.

```
xsdir            xsdir_new
        new_lib 2
C:\Users\m180078\my__mcnp\new_lib2
ZZAAA.##c
99999.99c      1300   99999.82c      99999.83c
#new_ZAID   new_Temperature    lower_bound_ZAID   upper_bound_ZAID
```

Figure C.1: Example SPECS File

The example specs file establishes in the first line two things, where the cross sections are being taken from (xsdir) and the name of the new cross section file (xsdir_new). In the next line, the specs file names the library and establishes the library as a type 2 library. This means that the library is in binary and not able to be read by human eyes. A type 1 library is capable of being read by human eyes, but runs much slower than a type 2. Finally, the specs file indicates the location of the new library and gives a path to that library. Once these steps are completed, one can begin to list the necessary cross sections in the specs file. The fourth line in Figure C.1 shows ZZAAA.##c as an example of an existing cross section being added to the library. The fifth line in Figure C.1 shows the process of Doppler broadening, which is described in the final line of Figure C.1. In order to create a new cross section through Doppler broadening, the first step is to name the new cross section with a unique identifier. An important note is that this identifier cannot exceed two numbers. Once the identifier is decided upon, the new temperature is stated and the existing cross sections that act as upper and lower bounds are added as shown in

Figure C.1. A list of existing cross sections can be found in various PDF files located in the MCNP_DATA/DATA_REF folder downloaded onto a workstation that has previously downloaded the MCNP package. This process is repeated for all desired temperatures and cross sections. In addition, one can also create multiple different libraries within the singular cross section directory on one specs file. This is done by creating a line of space after the last cross section in the first library and repeating the process of naming a library, including providing the type and path to that library.

There may be mistakes in the specs file that will stop makxsf from running. Things to ensure are that all stated cross sections and cross sections acting as upper/lower bounds exist. Some may be said to exist, but may not be able to be found when attempting to run makxsf. The only way to test this is by running the specs and seeing what cross sections the error appears at.

Once the specs file is created, the final step in creating these cross sections is to place the specs file in the operating directory and run the command *makxsf*. The *makxsf* command will search for a file named specs and begin to run the file by organizing all the cross sections and completing the Doppler broadening cross sections. This will create the desired cross section directory and library in the stated path. In order to use this new cross section directory when running a model, a simple command of *xsdir=xsdir_new* is added to the command run line. An example command line would be:

mcnp6 name=input_file.txt xsdir=xsdir_new

This tells MCNP to use the stated cross section directory, rather than the default cross section directory.

Appendix D: BURN Card Description

A burn card is how MCNP calculates burnup within a criticality calculation. An example burn card is shown below in Figure D.1.

```
burn time=365 6R power=1 mat=11 bopt=1.0 1 1
              pfrac=1.0 6R
              omit=11, 1, 6014, 11, 1, 6012, 11, 1, 6013,
                   11, 1, 7016, 11, 1, 8018, 11, 1, 9018,
                   11, 1, 10020
              matvol=47037.8592
```

Figure D.1: Burn Card Example

Names and descriptions of different pieces of the burn card are shown in Table D.1 below.

Table D.1: Burn Card Option Descriptions [20]

Burn Card Option	Example	Description
Time	time=i j k	i, j, and k represent the amount of time in days for time steps in between calculation of the k_{eff}. Each of the listed numbers indicate the amount of days for each time step
Power	power=x	This sets the power of the reactor in question to x number of megawatts
Material	mat=XX	This establishes what material is being subjected to burnup (typically the fuel)
Power Fraction	pfrac=X.X	This establishes for each timestep, what fraction of power is present. Must have same amount of responses as time.

Table D.1 (cont.): Burn Card Option Descriptions [20]

Burn Card Option	Example	Description
Omit	omit=m, n, o	This gives the option to omit certain isotopes from being created. The options represent the following: m: the material it is being omitted from n: number of isotopes o: the ZAID number of the isotope to be omitted
Material Volume	matvol=XXXX	This gives the total volume of material being subjected to burnup
Burnup Options	bopt=i j k	This gives different options to the user. The options include: i: Q value multiplier, multiplies with the value of power j: Tens digit controls what tier of burnup variables are reported (1, 2, or 3), the ones digit controls order of output (whether it's based on mass, total activity, specific activity, or ZAID) k: controls how MCNP will respond if there is not data for isotopes chosen

The example burn card shown in Figure D.1 shows that the k_{eff} will be calculated first after 365 days, and then repeating the calculation after 6 more time steps of 365 days. This means the final k_{eff} calculation will be done on the reactor after 7 years of use. The power option of the example shows that the reactor is being run at 1 MWt of power. The material used in the example is material 11, which is UO_2 in the code this excerpt is from. The example shows the burnup options to have a power multiplier of only 1. The burnup output will only include tier 1

variables and will list that in order of largest atomic mass to smallest. The last burn option indicates the code will calculate use data tables to calculate the value if the cross section is not in the cross section library. The example shows that all 7 time steps are run at a power fraction of 1.0, at 1 MW. If a 0.5 were listed, this would indicate that the time step correlating to the 0.5 listed would be run at half power. There must be an equal amount of power fractions to time steps listed with the example having 7 of each. The omitted isotopes are for material 11 and include C-12, C-14, and many others.

An important clarification from the previous paragraph is the tier of burnup variables. In total, there are three tiers of burnup variables. The higher tiers include isotopes that are created at lower probabilities. This study employs tier 1 isotopes as the other tiers include isotopes that are at a negligible concentration.